

**Investigation of the
X(5)–Structure in ^{176}Os
using Absolute Transition
Probabilities**

Inaugural-Dissertation
zur
Erlangung des Doktorgrades
der Mathematisch-Naturwissenschaftlichen Fakultät
der Universität zu Köln

vorgelegt von
Barbara Melon
aus Torre del Greco, Neapel, Italien

Köln 2011

Berichterstatter:

Prof. Dr. Jan Jolie
Priv.-Doz. Dr. Alfred Dewald

Tag der mündlichen Prüfung:

25th Januar 2011

Abstract

The investigation of the X(5) symmetry in a different mass region from the well established $A \approx 150$ region is a very actual topic in nuclear physics. The first example of an X(5) like nucleus, namely ^{178}Os , outside the $A \approx 150$ mass region has been found by Möller et al. [8, 51]. From the energy spectrum, the neighbor nucleus ^{176}Os is considered as a good candidate for a nucleus where the critical point symmetry X(5) [2] can be observed.

The aim of this work is to test the model predictions based on the X(5) critical point symmetry in the ^{176}Os nucleus. Reliable and precise lifetimes of excited states in ^{176}Os have been measured for the first time using the Recoil Distance Doppler Shift Method. Lifetime experiments were performed at the GASP array, INFN Legnaro and at the FN Tandem accelerator of the University of Cologne in combination with the Cologne plunger apparatus.

In ^{176}Os , the lifetime of eleven excited states were determined using the Differential Decay-Curve Method. In addition, the lifetime of excited states in ^{177}Os were measured. These states were populated in a weaker reaction channel. In addition two dedicated experiments were performed to remeasure the lifetime of the first excited 2^+ states in $^{176,178}\text{Os}$. The aim was to reduce the uncertainty of the $B(E2; 2_1^+ \rightarrow 0_1^+)$ values, which are normally used to normalize transition strength within a nucleus for the comparison with theoretical models.

The comparisons between the experimental transition quadrupole momenta Q_t of ^{176}Os derived from the experimental $B(E2)$ strengths and the predictions of the X(5) model confirm the consistency of an X(5)-like description of this nucleus.

Kurzzusammenfassung

Die Untersuchung der X(5) Symmetrie außerhalb der Massenregion um $A \approx 150$ ist ein sehr aktuelles Thema der Kernphysik. Das erste Beispiel hierfür wurde von Möller gefunden [8, 51] in ^{178}Os . Aus dem Energiespektrum kann man erkennen, dass auch der Nachbarkern ^{176}Os ein guter Kandidat für die Untersuchung der kritischen Punktsymmetrie X(5) [2] ist. Zuverlässige und präzise Lebensdauern der angeregten Zustände in ^{176}Os wurden zum ersten Mal mit der Recoil Distance Doppler Shift-Methode gemessen. Experimente zur Lebensdauer wurden an dem GASP Array am INFN Legnaro und an dem FN Tandem Beschleuniger der Universität zu Köln in Kombination mit der Kölner Plunger Apparatur durchgeführt.

In ^{176}Os wurde die Lebensdauer von 11 angeregten Zuständen mit der Differential Decay Curve-Methode bestimmt. Zusätzlich konnten die Lebensdauer der angeregten Zustände in ^{177}Os gemessen werden. Diese Zustände wurden in einem schwächeren Reaktionskanal bevölkert. Um die Lebensdauer der ersten angeregten 2^+ Zustände in $^{176,178}\text{Os}$ zu vergleichen, wurden zwei separate Experimente durchgeführt. Ziel war es, die Unsicherheit der $B(E2; 2_1^+ \rightarrow 0_1^+)$ Werte zu reduzieren. Diese Werte werden zur Normalisierung der Übergangsstärken vor dem Vergleich mit den theoretischen Modellen benutzt.

Die Vergleiche zwischen den experimentellen Quadrupol-Übergangsmomenten Q_t von ^{176}Os bestimmt aus den experimentellen $B(E2)$ Stärken und die aus dem X(5)-Modell abgeleiteten Vorhersagen bestätigen die Konsistenz einer X(5)-Beschreibung dieses Kerns.

To my father and my mother

Contents

Contents	i
List of Figures	1
List of Tables	5
Introduction	9
1 Theoretical background	11
1.1 The Geometrical model	12
1.1.1 The rotational model	13
1.1.2 The General Collective Model	14
1.2 The Interacting Boson Model	15
1.3 Phase transitions and X(5) symmetry	18
1.3.1 The X(5) symmetry: Iachello's solution	19
1.3.2 The exact numerical solution for the X(5) Hamiltonian: Caprio's solution	21
2 Lifetime measurement in the picosecond region	25
2.1 The RDDS Method	25
2.2 The Differential Decay Curve Method	27
2.2.1 The DDCM for coincidence measurements	29
3 Experimental details	31
3.1 The Plunger device	31
3.2 The GASP spectrometer	33
3.3 The ^{176}Os experiment at GASP	35
3.4 The $^{176,178}\text{Os}$ experiments at the Cologne FN Tandem accelerator	37
4 Data analysis	41
4.1 Calibration and Shift-correction	41
4.2 Distance calibration	42

4.3	Normalization	44
4.4	The recoil velocity	45
4.5	Application of the DDCM and the extraction of the lifetime	45
4.5.1	The lifetime τ	46
5	Experimental results	49
5.1	The experiment at GASP: ^{176}Os	50
5.1.1	Analysis of the ground state band	50
5.2	Lifetime of levels in the negative parity bands of ^{176}Os	53
5.2.1	Analysis of the first excited band	54
5.2.2	Analysis of the second excited band	55
5.3	The experiment at the Tandem in Cologne: lifetime of the first excited 2^+ in $^{178,176}\text{Os}$	56
5.3.1	Lifetime of the 2^+ state in ^{178}Os	57
5.3.2	Lifetime of the 2^+ state in ^{176}Os	57
5.4	Lifetimes in ^{177}Os	58
6	Comparison with the models and discussion	61
6.1	The nucleus ^{176}Os	62
6.1.1	^{176}Os as X(5) nucleus	65
6.2	The comparison with the theoretical models IBA and GCM	72
6.3	The negative parity bands in ^{176}Os	80
6.4	The rotational band in ^{177}Os	82
	Conclusions	85
	A Cascade calculation	87
	B Lifetimes	89
	Bibliography	93

List of Figures

1.1	Lund convention plot. The plot gives a description of the nuclear shape in the plane (β, γ) . At the margin is indicated the axe of symmetry.	13
1.2	The extended Casten triangle [5]. The IBM dynamical symmetries are indicated with circles. The solid dot represents the second order transition between spherical (I), deformed oblate (II) and prolate(III) nuclei. The dashed lines correspond to first-order phase transitions.	19
1.3	Schematic representation of the lowest portion of the X(5) spectrum [2]. Energies are in units of the $E(2_1^+ \rightarrow 0_1^+) = 100$.The arrow thicknesses are full-scale adapted to the reduced transition probabilities.	20
1.4	Schematic representation of the exact X(5) solution [27]. Energies are in units of the $E(2_1^+ \rightarrow 0_1^+) = 100$. The arrow thicknesses are full-scale adapted to the reduced transition probabilities.	22
2.1	A schematic setup of an RDDS experiment.	26
2.2	Arbitrary decay and feeding pattern of level l_i	28
3.1	Drawing of the Cologne plunger apparatus [30].	32
3.2	A gold stopper foil is mounted and stretched on the aluminum cone.	32
3.3	The GASP spectrometer in open condition and for configuration C1. The picture shows the Cologne Plunger device as it is mounted in the spectrometer.	34

3.4	Spectra of transitions of ^{176}Os measured at distances of 5, 25 and $150\ \mu\text{m}$ with the detectors positioned at 34.6° with respect to the beam axis. The components of transitions in the gsb of ^{176}O which show the effect of the Doppler broadening are indicated with labels. The label U stands for the unshifted component and S for the shifted component.	38
3.5	Spectra of ^{178}Os measured at distances of 200, 1300 and $4000\ \mu\text{m}$ between the foils with the detector at 0 deg with respect to the beam axis. The two components of the $2_1^+ \rightarrow 0_1^+$ transition are indicated. The label U stands for the unshifted component and S for the shifted component.	39
3.6	Spectra of ^{176}Os measured at distances of 600, 2000 and $4000\ \mu\text{m}$ between the foils with the detector at 0 deg with respect to the beam axis. The two components of the $2_1^+ \rightarrow 0_1^+$ transition are indicated. The label U stands for the unshifted component and S for the shifted component.	39
4.1	Distance calibration of the RDDS for the ^{176}Os experiment. . .	43
4.2	Capacity of the system target-to-stopper at short distances. . .	43
4.3	Napatau graphical representation: Lifetime of the 6^+ in ^{176}Os . From the top to the bottom respectively: τ curve, the shifted intensity I_{sh} and in the last plot I_{un} is fitted simultaneously with the derivative $\tau \frac{dI_{sh}}{dx}$	48
4.4	Napatau graphical representation: Lifetime of the 4^+ in ^{176}Os	48
5.1	τ -plot and intensities of the shifted I_{sh} and unshifted I_{un} components of the transition $6_1^+ \rightarrow 4_1^+$ in ^{176}Os	52
5.2	τ -plot and intensities of the shifted I_{sh} and unshifted I_{un} components of the transition $4_1^+ \rightarrow 2_1^+$ in ^{176}Os	52
5.3	Partial level scheme of ^{176}Os [40]. The two side bands with negative parity which are investigated in this work are marked as neg-1 and neg-2.	60
6.1	Partial level scheme of ^{176}Os (gsb and β band) compared with the predictions of the $s = 1, 2$ bands of the X(5) model. Energies are in (keV) and normalized to the experimental $E(2^+)$ value.	63
6.2	Normalized energy levels of the yrast band for the $^{176,178}\text{Os}$, ^{150}Nd and ^{152}Sm . The values are compared with the predictions of the theoretical models. The experimental energies are taken from NDS	64

6.3	Transition quadrupole moments in the ground state band of ^{176}Os . The measured values are compared to the expected ones for the rigid rotor, the X(5)-like nucleus in the approximate case and the U(5) limit of the IBA.	67
6.4	Comparison of the Q_t -values in the gsb of ^{176}Os (a) with well known X(5)-like nuclei ^{154}Gd (c)[4] and the X(5)-like nucleus ^{178}Os [8, 51].	68
6.5	Experimental level scheme and B(E2) transition strengths (in e^2b^2) compared to the X(5)exact numerical solution. Energies presented are in keV.	70
6.6	. Experimental level scheme and B(E2) transition strengths (in e^2b^2) compared to the IBM-1 fit. Energies presented are in keV.	74
6.7	. Experimental level scheme and B(E2) transition strengths (in e^2b^2) compared to the GCM fit. Energies presented are in keV.	76
6.8	Experimental energy ratios (a) and the normalized experimental transition probabilities (b) for the ground state sequence (up to spin $j = 10$) in ^{176}Os are plotted versus spin together with those predicted by the X(5) model, IBM and GCM. The rotor and vibrator limits are also given for comparison.	78
6.9	experimental energy ratios (a) and the transition probabilities (b) of the X(5) like nuclei ^{178}Os and ^{176}Os , are plotted together with those of two well known X(5)-like nuclei, ^{150}Nd [6] and ^{152}Sm [20].	79
6.10	Projection of the GCM potential $V(\beta, \gamma)$ for ^{176}Os with $\gamma = 0^\circ$, 30° and 60° . The position of the ground state is indicated by the horizontal line.	80
6.11	Projection of the GCM potential $V(\beta, \gamma)$ for ^{154}Gd [4, 51] with $\gamma = 0^\circ$, 30° and 60° . The position of the ground state is indicated by the horizontal line.	80
6.12	γ dependence of the GCM potential $V(\beta, \gamma)$ for ^{176}Os for β value corresponding to coordinates of the absolute potential minimum.	81
6.13	γ dependence of the GCM potential $V(\beta, \gamma)$ for ^{154}Gd [4, 51] for β value corresponding to coordinates of the absolute potential minimum.	81
6.14	B(E2)-values of intraband transitions within the negative parity band neg-1. The lines connect the values obtained by means of eq. 6.1 for fixed values of $K_{rms} = \sqrt{\langle K^2 \rangle}$	83

6.15	Comparison of the PTRM calculations performed by P. Petkov with the experimental data in ^{177}Os [51]. The $B(E2)$ values from [51] are given between the levels. The band under investigation in the present work is indicated with $\nu 1/2[521]$ and the levels observed are marked with arrows.	84
A.1	Cascade calculation [35] for the reaction $^{152}\text{Sm}(^{29}\text{Si}, 4n)^{176}\text{Os}$.	87
A.2	Cascade calculation [35] for the reaction $^{164}\text{Er}(^{16}\text{O}, 4n)^{176}\text{Os}$.	88
A.3	Cascade calculation [35] for the reaction $^{164}\text{Er}(^{16}\text{O}, 4n)^{176}\text{Os}$.	88

List of Tables

1.1	Energies and transition strengths of the approximate X(5) model for the bands $s = 1$ and $s = 2$ [2, 25]. Energies are in units of the $E(2_1^+ \rightarrow 0_1^+) = 100$. Transition rates are also reported fixing $B(E2; 2_1^+ \rightarrow 0_1^+) = 100$	21
1.2	Energies of the exact X(5) solution for the gsb as well as for the β and γ bands as reported in the tabulations [27, 28] for $a = 200$. Energies are in units of $E(2_1^+ \rightarrow 0_1^+) = 1$	23
1.3	Comparison of the predicted energies and transition probabilities for the $s = 1$ (gsb) band of the approximate [2] and exact X(5) solution. The energies and transition probabilities of the exact X(5) solution for the $s = 1$ are extracted from the tabulations [27, 28] for $a = 200$. Energies are in units of $E(2_1^+ \rightarrow 0_1^+) = 1$ and transition rates are reported fixing $B(E2; 2_1^+ \rightarrow 0_1^+) = 1$	23
3.1	Distribution of the 40 HPGe detectors of GASP over 7 rings.	35
3.2	Technical details of the plunger experiment at GASP.	36
3.3	Technical details of the experiments at the FAN tandem, Cologne.	40
4.1	Normalization factors $N(d)$ for the ^{176}Os measurement at LNL. These values are valid for all the GASP rings used in the analysis.	44
5.1	Lifetimes of levels in the gsb of ^{176}Os at each ring–ring combinations. The first column indicates the gate used to determine these values. The label YYYSH indicates that the gate is set on the shifted component of the transition YYY.	53
5.2	Lifetimes of levels in the gsb of ^{176}Os . The lifetime τ_{corr} corrected for the slowing down of the recoils in the stopper material is reported. In the last column the lifetimes known in literature τ_{lit} [9] are reported.	54

5.3	Lifetimes of levels in the two negative parity bands of ^{176}Os at each ring–ring combinations. The first column indicates also the gate used to determine these values. The label YYYYSH indicates that the gate is set on the shifted component of the transition YYY	55
5.4	Lifetimes of levels in the first and second excited band of ^{176}Os . The other data are taken from Nuclear Data. Sheets	56
5.5	Lifetimes of the first excited 2^+ of $^{176,178}\text{Os}$. The experimental results are compared with the lifetime τ_{lit} measured by O. Möller [3] and the lifetimes τ_{ee} measured with the Double Orange [50].	57
5.6	Measured lifetimes and transition probabilities in the ground state band of ^{176}Os . The other data are taken from Nuclear Data Sheets.	58
5.7	Measured lifetimes of the first excited $\frac{9}{2}^-$, $\frac{13}{2}^-$ and $\frac{15}{2}^-$ states in ^{177}Os . The experimental results are compared with the lifetime τ^\dagger measured by O. Möller [51]. The other data are taken from the Nuclear Data Sheets	59
6.1	Energy ratios of levels in the gsb of ^{178}Os and ^{176}Os with the corresponding X(5) values. All the values are relative to the energy of the 2^+ . The energy values are taken from NDS [52].	63
6.2	$B(E2; I \rightarrow I - 2)$ normalized to the $B(E2; 2_1^+ \rightarrow 0_1^+)$	63
6.3	Comparison of the energy ratios of levels in Os isotopes to the prediction of the X(5) model and to the known X(5)–like nuclei ^{154}Gd [4] and ^{152}Sm [20].	65
6.4	Comparison of the relative transition probabilities of the X(5) predictions from [2] with the experimental values in $^{176,178}\text{Os}$. The intensities are normalized to the intensity of the transition $I_2^+ \rightarrow (I - 2)_2^+$. The γ –intensities are taken from [53].	66
6.5	Comparison of the relative transition intensities of the exact numerical X(5) † and approximate X(5) predictions [2, 27] with the experimental values in ^{176}Os . The γ –intensities for the interband transitions are taken from [53].	71
6.6	The relative transition probabilities of transition between the β , γ and gsb in ^{176}Os . The intensities are normalized to the intensity of the strongest transition. The experimental γ –intensities are taken from [53].	73
6.7	Parameters of the IBM–1 and GCM fits for ^{176}Os	77

6.8	Casten triangle for parameters of IBM-1. The position of the ^{176}Os nucleus is indicated. In the table the parameters of the IBM-1 fit for ^{176}Os as well as the parameters which correspond to the X(5) symmetry in the framework of IBM.	82
6.9	Comparison of $B(E2)^\dagger$ in ^{177}Os obtained from the PTRM calculations made by P.Petkov with the experimental $B(E2)$ calculated from lifetimes derived in this work and the experimental $B(E2)^\ddagger$ obtained in [51].	84
B.1	Lifetimes of levels in the gsb of ^{176}Os at each ring-ring combinations. In the first column is indicated also in correspondence of which gate the data are referring. The label YYYSH indicates that the gate is set on the shifted component of the transition YYY.	89
B.2	Lifetimes of levels in the gsb of ^{176}Os . The lifetime τ_{corr} corrected for the slowing down of the recoils in the stopper material is reported.	90
B.3	Lifetimes of levels in the two negative parity bands of ^{176}Os at each ring-ring combinations.	90
B.4	Lifetimes of levels in the first and second excited band of ^{176}Os	91
B.5	Lifetimes of the first excited 2^+ of $^{176,178}\text{Os}$	91
B.6	Measured lifetimes and transition probabilities in the ground state band of ^{176}Os	92
B.7	Measured lifetimes of levels in ^{177}Os	92

Introduction

Critical point symmetries describing nuclei at the point of shape transitions between different limiting symmetries are an attractive topic in nuclear structure. The symmetries X(5) [2] and E(5) [1] at the critical point of phase transition from spherical nucleus to axial deformed rotor and from spherical to triaxial γ soft deformed nucleus, respectively, have been introduced by F. Iachello. A lot of theoretical and experimental work has been devoted to these topics, especially focussed on how the phase transitions manifest in nuclei [3, 4, 6, 18]. In particular J. Jolie interprets these symmetries with the Landau theories of the phase transition [5] at the critical point.

The success of the X(5) model in describing the properties of some nuclei is in its parameter free predictions which allows to compare directly the energy spectrum and the transition rates. Only two scaling factors are taken in consideration for the comparison with the experimental data. The first nuclei which have been described by the X(5) model are located in the mass region $A \approx 150$: ^{150}Nd [6], ^{152}Sm [7] and ^{154}Gd [4]. The search for X(5) candidates in a different mass region is a very actual topic in nuclear physics. Indeed, since the first $N=90$ isotons were described in the frame of the X(5) model, other candidates were searched in other mass regions. In order to find other X(5) regions where X(5)-like nuclei can be found, it appears reasonable to look where fast transitions from spherical to axially symmetric deformation are expected. Thus regions around mid-shell for nucleons of one type with few valence of nucleons of the other type are the most promising ones for finding X(5) type nuclei [8].

In the $A \approx 180$ mass region, it has been shown that ^{178}Os exhibits the characteristic features predicted by the X(5) model [8]. It represents the first example of an X(5)-like nucleus identified outside the well established $A \approx 150$ mass region. On the basis of the excitation energy pattern the neighboring isotope ^{176}Os can also be considered as a good X(5) candidate. However, transition probabilities, which provide a crucial test for shape changes, have to be measured to be able to draw definite conclusions. The lifetime of the 2_1^+ [3] state and from the 8_1^+ state up to the 20_1^+ [9] in ^{176}Os are known from

literature. At the time we performed our experiment only the lifetime of the 2_1^+ [3] state was known. The lifetime of the 8_1^+ and the 10_1^+ states measured by us have more recently also been remeasured by an independent group [9].

Therefore, an experiment was performed to measure lifetimes of low-lying excited states in ^{176}Os using the Köln coincidence plunger device and the GASP spectrometer at the Laboratori Nazionali di Legnaro. Excited states in ^{176}Os were populated via the $^{152}\text{Sm}(^{29}\text{Si},5n)^{176}\text{Os}$ reaction at $E(^{29}\text{Si}) = 150\text{ MeV}$. With the high γ efficiency GASP spectrometer it was possible to observe also weakly populated levels in side bands. The use of the Cologne plunger device with an automatic feedback system for the correction of the target-to-stopper distance ensures high precision measurements. The Differential Decay Curve Method has been applied to extract the lifetimes from the data. The E2 transition probabilities, calculated from the experimental lifetimes, are crucial for the investigation in phase transition together with the energies of levels in the ground state band and in the γ and β bands. The comparison of the experimental $B(E2)$ values and the energy spectrum with the theoretical predictions allows an interpretation of the ^{176}Os as an X(5) nucleus.

In the first chapter of this thesis a brief overview of the theoretical nuclear models used for the interpretation of the nuclear structure of the nucleus under investigation is given. In the second chapter the experimental technique used in the experiment is described. A briefly description of the analysis method is also given. A description of the experimental setup, e.g. the GASP spectrometer and the Cologne plunger device, is done in the third chapter as well as the details of the experiment performed in order to measure lifetimes in ^{176}Os . The fourth chapter contains details about the steps of the data analysis which lead to the extraction of the lifetimes. The experimental results obtained from the analysis of the data are summarized in the fifth chapter. In particular a full description of the determination of each single lifetime measured in these experiments is given, specifying the uniqueness of each case. In the sixth and last chapter the comparison of the experimental results presented in fifth chapter and the outcome of the theoretical models predictions described in first chapter is discussed.

Chapter 1

Theoretical background

In this chapter the nuclear models used for the interpretation of the nuclear structure in the mass region $A \sim 180$ are presented.

A nuclear model represents an instrument to describe the structure of the nucleus. Models are simplified descriptions of physical systems which would be impossible to treat exactly. A good model tries to identify a few important degrees of freedom of the system to reproduce reasonably well the observed data.

The complexity of the nuclear system requires that in the nuclear landscape (along the nuclear chart) different models are necessary for the interpretation of the different structures observed experimentally. As I. Talmi observed [10] ” *Still a good model sometimes works well even where apparently it is not valid. This is in contrast to bad models which are useless even where they are supposed to work*”. It happens sometimes that regions of validity of two different models overlap, so that the nucleus itself can be well described by two different models.

To describe very light nuclei and those with very near closed shells the *Shell Model* is widely used. Indeed, to describe nuclei far from closed shells the use of the shell model becomes intractable since the size of the matrices in which the residual interaction must be diagonalized becomes rapidly enormous. The description of nuclei far from doubly closed shells is done making use of a macroscopic approach. The so called *geometrical* or *collective model* successfully describes collective motions of nucleons. In the framework of this model the nuclear structure of heavy nuclei can be described in terms of more effective degrees of freedom, the *collective variables*.

Collective models are classified as *geometrical* or *algebraic*.

Fortunately, low-lying spectra of nuclei away from closed major shells indeed show a relatively simple structure, related to the occurrence of collective phenomena, which can be described in terms of collective parameters. It

turns out that their spectra can be arranged into bands of collective states. The members of such a band are connected by strong electric quadrupole (or M1) transitions.

A small overview of the nuclear models used for the interpretation of the experimental results of this work is given in the following sections.

1.1 The Geometrical model

In the framework of the Geometrical Model, introduced by A. Bohr and B. R. Mottelson in 1952 [11], the nucleus is seen as a geometrical body with a well defined surface and homogeneously distributed mass and charge density. In this geometrical model the nucleus is assumed to be able to undergo small surface and shape oscillations. The presence of a deformation in the nucleus implies in general the existence of an intrinsic quadrupole momentum Q_0 which illustrates the deviation of the charge distribution from a spherical form. One usually considers the quadrupole deformation as the most important mode of collective motion.

The intrinsic Q_0 can be determined from reduced transition probabilities of a transition of the rotational band and characterizes the shape of the nucleus. In this model the nucleus is assumed as a droplet described by a set of collective coordinates α . The equation of the nuclear surface can be written as

$$R(\theta, \phi) = R_0 \left[1 + \sum_{\lambda} \sum_{\mu} \alpha_{\mu}^{\lambda} Y_{\lambda, \mu}^*(\theta, \phi) \right], \quad (1.1)$$

where α_{μ} are the components of an irreducible tensor of rang λ , R_0 the radius of a sphere of the same volume ($1.2 \text{ fm } A^{1/3}$). Since the dominant type of nuclear deformation is a quadrupolar deformation, the sum can be with good approximation restricted just to terms with $\lambda = 2$. Under this approximation and using the Hill-Wheeler coordinates β and γ which are related to the α_{μ} components as

$$\alpha_{20} = \beta \cos \gamma, \quad \alpha_{22} = \alpha_{2-2} = \frac{1}{\sqrt{2}} \beta \sin \gamma, \quad \alpha_{21} = \alpha_{2-1} = 0, \quad (1.2)$$

the equation 1.1 becomes:

$$R_k = R_0 \left[1 + \sqrt{\frac{5}{4\pi}} \beta \cos \left(\gamma - \frac{2\pi}{3} k \right) \right], \quad (1.3)$$

with $k = 1, 2, 3$. The parameter β gives a measure of the deformation while the γ characterizes the nuclear shape. Each couple of variables (β, γ) defines a particular nuclear shape as shown in fig. 1.1

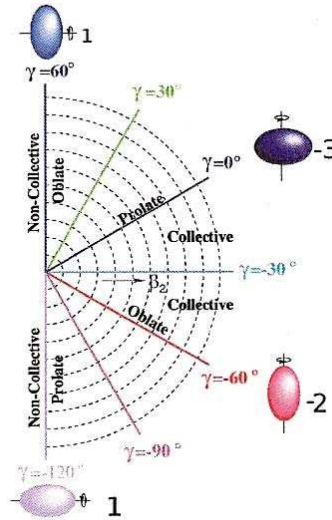


Figure 1.1: Lund convention plot. The plot gives a description of the nuclear shape in the plane (β, γ) . At the margin is indicated the axe of symmetry.

In particular for β positive and γ in the interval between 0° and 60° the nucleus is defined by these two parameters as follow

$$\begin{aligned}
 \gamma = 0^\circ & & : & \text{prolate deformation around the 3-rd axis(axial symm. nucleus),} \\
 \gamma = 60^\circ & & : & \text{oblate deformation around the 2-nd axis (axial symm. nucleus),} \\
 0^\circ < \gamma < 60^\circ & & : & \text{triaxial deformation (axial asymmetric nucleus),} \\
 \beta = 0 & & : & \text{spherical nucleus.}
 \end{aligned}
 \tag{1.4}$$

1.1.1 The rotational model

This collective nuclear model is based on the assumption that the nucleus presents an axial symmetric deformation of the ground state. The main degree of freedom is a collective rotation of the nucleus with respect to an axis orthogonal to the symmetric axis. The excitation energies of the rotational band is given by

$$E_{rot} = \frac{\hbar}{2\mathfrak{I}}[I(I+1) - K^2], \quad (1.5)$$

where I is the total angular momentum of the nucleus, \mathfrak{I} is the inertial momentum of the nucleus and K is the projection on the symmetry axis of I . In this framework the reduced transition probabilities are expressed in terms of the intrinsic quadrupole momentum Q_0 as

$$\begin{aligned} B(E2; I+2 \rightarrow I) &= \frac{5}{16\pi} Q_0^2 \langle (I+2)K20 | IK \rangle, \\ &= \frac{5}{16\pi} Q_0^2 \frac{3}{2} \frac{(I+1)(I+2)}{(2I+3)(2I+5)}, \end{aligned} \quad (1.6)$$

The intrinsic quadrupole momentum Q_0 is given as function of the deformation parameter β [11] as

$$Q_0 = \frac{3}{\sqrt{5\pi}} Z R_0^2 \beta \left(1 + \frac{1}{8} \sqrt{\frac{5}{\pi}} \beta + \frac{5}{8\pi} \beta^2 + \dots \right), \quad (1.7)$$

with $R_0^2 = 0.0144 A^{\frac{2}{3}} b$ and Q_0 in [eb].

As predicted by the rigid axial symmetric rotor model one would expect that the quadrupole momentum Q_0 inside a rotational band is constant. In the framework of this model the transition quadrupole momentum Q_t is defined by the relationship

$$B(E2; I+2 \rightarrow I) = \frac{5}{16\pi} Q_t^2 \langle (I+2)K20 | IK \rangle. \quad (1.8)$$

1.1.2 The General Collective Model

The Geometrical Collective Model (GCM) of Gneuss and Greiner [12] provides a description of nuclear quadrupole surface excitations using a Schrödinger-like Hamiltonian. This phenomenological model gives a geometrical representation of the nuclear shape of low-lying levels in even-even nuclei.

The Hamiltonian is expressed as series expansion in terms of surface deformation coordinates $\alpha_{2\mu}$ and the conjugate momenta $\pi_{2\mu}$ with

$$[\hat{\pi}_{2\nu}, \alpha_{2\mu}] = -i\hbar\delta_{\mu\nu}.$$

$$\hat{H} = \frac{1}{B_2} [\pi \times \pi]^{(0)} + B_3 [[\pi \times \alpha]^{(2)} \times \pi]^{(0)} + \dots + C_3 [\alpha \times \alpha]^{(0)} + C_3 [[\alpha \times \alpha]^{(2)} \times \pi]^{(0)} + \dots \quad (1.9)$$

The terms in π may be classified as kinetic energy or as potential energy for the terms involving only the coordinates α .

The Hamiltonian in Eq. 1.9 reduces to the Schrödinger-like Hamiltonian if the kinetic term is restrained to the lowest order of the expansion. This truncated Hamiltonian can be shown to be equivalent to the Bohr Hamiltonian [11]. The potential energy depends only on the shape of the nucleus and can be expressed in terms of the Bohr Hamiltonian shape coordinates β and γ as

$$\begin{aligned}
 V(\beta, \gamma) = & \frac{2}{35}C_6\beta^6 \cos 3\gamma^2 & (= V_{NA}(\beta, \gamma)) \\
 & + \frac{1}{\sqrt{5}}C_2\beta^2 + \frac{1}{5}C_4\beta^4 + \frac{1}{5\sqrt{5}}D_6\beta^6 & (= V_S(\beta)) \\
 & - \sqrt{\frac{2}{35}}C_3\beta^3 \cos 3\gamma - \sqrt{\frac{2}{175}}C_5\beta^5 \cos 3\gamma & (= V_{PO}(\beta, \gamma)) \\
 & + \dots
 \end{aligned} \tag{1.10}$$

The GCM Hamiltonian with eight parameters ($B_2, B_3, C_2, C_3, C_4, C_5, D_6$), which are estimated by fitting experimental data, is capable to describe a rich variety of nuclear structures.

The terms with constants C_2, C_4 and D_6 are the γ -independent part of the potential, $V_S(\beta)$. The triaxial nuclear shapes are described by the term with C_6 which is symmetric with respect to $\gamma = 30^\circ$ ($V_{NA}(\beta, \gamma)$). The terms C_3 and C_5 characterize the oblate and the prolate nuclear shape, $V_{PO}(\beta, \gamma)$.

1.2 The Interacting Boson Model

In the previous section the collective spectra of a nucleus have been described using a geometrical model. Alternatively, algebraic models can be used for the same purpose. In 1974 A. Arima and F. Iachello [13–16] proposed a new nuclear model called *The Interacting Boson Approximation* (IBA). The basic idea is to assume that low-lying collective states in medium and heavy even-even nuclei can be described by a system of interacting s and d bosons carrying angular momentum 0 and 2, respectively.

In the simplest version of the Interacting Boson Approximation Model (IBA – 1) the low-lying collective states are dominated by excitation of the valence protons and neutrons while the closed-shell core is inert. It is assumed that the dominant particle configurations contributing to the nuclear shape of the low-lying states are those with identical particles coupled to pairs of

angular momentum 0 or 2. In the IBA - 1 the difference between protons and neutrons is neglected. The number of bosons is obtained counting from the nearest closed shells.

In second quantization, mostly the IBA Hamiltonian in multipole expansion is used, in which the relation of each term to the nuclear structure stands out more clearly. In this parameterization the boson-boson interactions are grouped so that the Hamiltonian takes the form:

$$H = \epsilon \hat{n}_d + a_0 \hat{P}^\dagger \cdot \hat{P} + a_1 \hat{L} \cdot \hat{L} + a_2 \hat{Q} \cdot \hat{Q} + a_3 \hat{T}_3 \cdot \hat{T}_3 + a_4 \hat{T}_4 \cdot \hat{T}_4, \quad (1.11)$$

where the dot stands for scalar product

$$\begin{aligned} \hat{n}_d &= \sqrt{5}(d^\dagger \cdot \tilde{d})^{(0)} && \text{the boson number operator,} \\ \hat{P} &= \frac{1}{2}(\tilde{d} \cdot \tilde{d} - s \cdot s) && \text{the pairing operator,} \\ \hat{L} &= \sqrt{10}(d^\dagger \tilde{d})^{(1)} && \text{the angular momentum operator,} \\ \hat{Q} &= (d^\dagger s + s^\dagger \tilde{d}) - \frac{\sqrt{7}}{2}(\tilde{d} \cdot \tilde{d})^{(2)} && \text{the quadrupole operator,} \\ \hat{T}_3 &= (d^\dagger \tilde{d})^{(3)} && \text{the octupole operator,} \\ \hat{T}_4 &= (d^\dagger \tilde{d})^{(4)} && \text{the hexadecapole operator,} \end{aligned} \quad (1.12)$$

with s^\dagger , s , d_μ^\dagger and d_μ with $\mu \in -2, -1, 0, 1, 2$ are the creation and annihilation operators of s and d bosons. The operator s^\dagger creates a boson in the $l = 0$ state. The operator d_μ^\dagger creates a boson in the $l = 2$ state with $l_z = \mu$. The corresponding annihilation operators are the hermitian conjugates s and d_μ . The operators d_μ^\dagger transform under rotation like the components of an irreducible tensor of rank $l = 2$ and the operator d_μ annihilates a boson with $l = 2$, $l_z = \mu$ and, a part of a phase factor, is $-\mu$ component of an irreducible tensor of rank $l = 2$. The phase factor is given by

$$\tilde{d}_\mu = (-1)^\mu d_{-\mu}, \quad (1.13)$$

The characteristics of the IBA are founded in the principles of the group theory. Since the s boson ($l = 0$) has only one magnetic substate and a d boson ($l = 2$) has 5 magnetic substates, the system s-d boson can be looked at, from the mathematical point of view, as a six dimensional space. The five magnetic substates of the d boson ($\mu \in -2, -1, 0, 1, 2$) and the

single substate of the s boson can be regarded as forming a six-dimensional vector space $U(6)$. In the $U(6)$ group there are 36 possible bilinear operator combinations that satisfy the conservation of the boson number,

$$s^\dagger s, s^\dagger \tilde{d}_\mu, d_\mu^\dagger s, (d^\dagger \tilde{d})_\mu^{(l)} \quad l=0,1,2,3,4 \quad (1.14)$$

$$\mu = +4, +3, \dots, -3, -4 \quad |\mu| \leq l$$

which form a closed set under commutation. This set of operators of the group of transformation $U(6)$ is said to form the Lie algebra $U(6)$. The operator which commutes with all the generators of the group is called the *Casimir operator*. Such operator can be composed of linear or higher order combinations of the generators. The linear Casimir operator of $U(6)$ is a total boson number operator $C_{1U(6)} = \hat{N} \equiv (d^\dagger \cdot \tilde{d})^{(0)} + s^\dagger s$. Inside the $U(6)$ algebra it is possible to find some sub-algebras which are characterized by a smaller set of the 36 generators which themselves close on commutation. One example, the 25 generators $(d^\dagger \tilde{d})_\mu^{(l)}$ are the generators of the $U(5)$ subgroup of $U(6)$. The Casimir operator of this group is the operator \hat{n}_d .

In this way it is possible to build a chain of groups and subgroups starting from $U(6)$ and ending with $O(3)$. For each of these chains the Hamiltonian is written as sum of the Casimir operators of the subgroups. The solution of the eigenvalue problem for such a chain is reduced to that of finding the eigenvalues of each of the Casimir operators. If the entire Hamiltonian can be written in terms of the Casimir operators of the groups appearing in the group chain, we are in presence of a dynamical symmetry. It turns out that in the present case there are three possible chains of sub-algebras

$$U(6) \supset U(5) \supset O(5) \supset O(3) \quad U(5)\text{-limit}$$

$$U(6) \supset O(6) \supset O(5) \supset O(3) \quad O(6)\text{-limit} \quad (1.15)$$

$$U(6) \supset SU(3) \supset O(3) \quad SU(3)\text{-limit}$$

The geometrical interpretation of the Lie groups are also of interest. The $U(5)$ limit is appropriate to describe spherical or near-spherical nuclei, where vibrations are the major mechanism of excitation. The $O(6)$ limit corresponds to a γ -soft rotor, a deformed nucleus with γ -instability. The $SU(3)$ limit corresponds to an axial symmetric rigid rotor.

1.3 Phase transitions and X(5) symmetry

In nuclear physics the phase transitions correspond to a shape transition [17] similar to those observed in crystal structures by varying the temperature. As J. Jolie *et al.* [5] pointed out "the Landau theory of continuous phase transitions, constructed almost 70 years ago for infinite classical system, is shown to be a useful approach also for finite quantal systems such as an atomic nucleus". In analogy to the classic theory of phase transitions, it is necessary to find a control parameter, which assumes a specific value at the critical point and which allows the identification of the phase transition of the system. The control parameter characterizes an observable which constitutes the order parameter. The concept of the phase transitions within the framework of the interacting boson approximation (IBA) model can be studied through the coherent state formalism. In this framework, a standard two-dimensional parameterization of the IBM-1 Hamiltonian is

$$\hat{H}(N, \eta, \chi) = \eta \hat{n}_d + \frac{\eta - 1}{N} \hat{Q}_\chi \cdot \hat{Q}_{\chi'} \quad (1.16)$$

where $\hat{n}_d = d^\dagger \cdot \tilde{d}$ is the d-boson number and $\hat{Q}_\chi = (d^\dagger s + s^\dagger \tilde{d})^{(2)} + \chi (d^\dagger \times \tilde{d})^{(2)}$ the quadrupole operator [61]. N is the total number of bosons. The control parameter η and χ vary within the range $\eta \in [0, 1]$ and $\chi \in [-\sqrt{7}/2, \sqrt{7}/2]$. In the parameter space, this can be represented as an extended Casten triangle [5, 18] – see Fig. 1.2. The parameter value $\eta = 1$ corresponds to the $U(5)$ dynamical symmetry, while the $SU(3)$ (prolate), $O(6)$ (γ -soft) and $\overline{SU}(3)$ (oblate) are located on the $\eta = 0$ axis in correspondence with the control parameter $\chi = -\sqrt{7}/2, 0, \sqrt{7}/2$, respectively.

The geometric interpretation of the Hamiltonian can be derived using the s-d boson condensate state $|N\beta\gamma\rangle$ defined in Ref. [19]. The energy functional $E(N, \eta, \chi; \beta, \gamma) = \langle N\beta\gamma | \hat{H}(N, \eta, \chi) | N\beta\gamma \rangle$ encodes several phase-transitional phenomena [20] described in general framework of the Landau theory [22]. The functional $E(N, \eta, \chi; \beta, \gamma)$ depends on the external parameters η and χ and on the order parameters β and γ . The task is to minimize the functional by varying the order parameters β and γ for each η and χ . Discontinuities in the first or second derivatives are observed in the first order or second order phase-transitions, respectively. In analogy to the classical theory of the phase transitions one can speak of critical point at the phase-transition and one can distinguish also with respect to parameter space of IBM between transitions of first and second order. A transition from spherical to gamma-soft nucleus is of the second order while a transition from spherical to axial symmetric deformed shape is a phase transition of the first order [23]. Recently, alternative descriptions of nuclei at the critical point of the

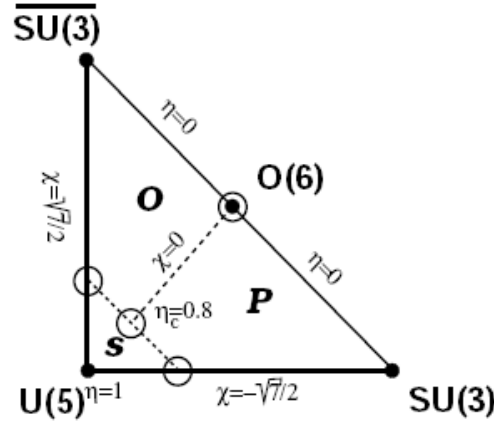


Figure 1.2: The extended Casten triangle [5]. The IBM dynamical symmetries are indicated with circles. The solid dot represents the second order transition between spherical (I), deformed oblate (II) and prolate(III) nuclei. The dashed lines correspond to first-order phase transitions.

phase transitions from spherical vibrator to deformed γ soft, E(5) [1], and from spherical vibrator to deformed axially d symmetric rotor, X(5) [2] have been proposed. These symmetries are not solved algebraically, but by computing the Bohr equation numerically for the potential at the critical point [24]. The essential point of these models is that at the critical point, the eigenvalue of the energy and the transition probabilities are fixed in a unique way by the symmetry. This allows one to scale the experimental values to the parameter-free prediction with a single scaling factor.

1.3.1 The X(5) symmetry: Iachello's solution

Critical point symmetries [1, 2] describe nuclei at points of shape/phase transitions between different limiting dynamical symmetries. Iachello proposed an approximate separation of variables for the Bohr Hamiltonian with a restoring potential $u(\beta, \gamma) = u(\beta) + u(\gamma)$ which decouples in terms of deformation variables. The solution involves a five-dimensional infinite square-well potential in the β collective variable and an harmonic oscillator potential in the γ variable to provides stabilization around $\gamma = 0$. The solution of the Bohr Hamiltonian under Iachello's approximation gives the energy of the levels in units of $E_{1,2} - E_{1,0}$. The notation is $E_{s,L}$ where s indicates the family label and L is the angular momentum and as example with $E_{1,2}$ is indicated the energy of the excited 2^+ state in the ground state band. Different families

are characterized by the energy ratio $R_s = \frac{E_{s,4} - E_{s,0}}{E_{s,2} - E_{s,0}}$. This ratio is 2.91 for $s = 1$ [2]. The location of the family $s = 2$ is given by the ratio $\frac{E_{2,0} - E_{1,0}}{E_{1,2} - E_{1,0}} = 5.67$ [2]. Figure 1.3 shows the schematic representation of the lowest portion of the X(5) spectrum.

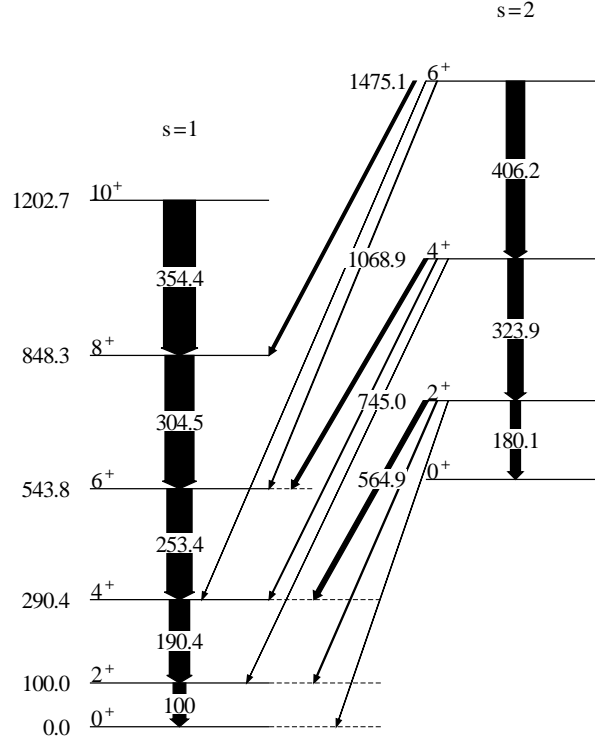


Figure 1.3: Schematic representation of the lowest portion of the X(5) spectrum [2]. Energies are in units of the $E(2_1^+ \rightarrow 0_1^+) = 100$. The arrow thicknesses are full-scale adapted to the reduced transition probabilities.

This theoretical spectrum is, with exception for scaling factors for the energy levels and for the transition intensities, a parameter free prediction and can be directly compared the experimental spectra.

In table 1.1 the energy and the transition strengths of the Iachello X(5) solution for the ground state band (gsb) and β band are summarized. This solution have been extensively compared with experimental data [4, 6, 8] and will be compared with the results obtained from this work.

Table 1.1: Energies and transition strengths of the approximate X(5) model for the bands $s = 1$ and $s = 2$ [2, 25]. Energies are in units of the $E(2_1^+ \rightarrow 0_1^+) = 100$. Transition rates are also reported fixing $B(E2; 2_1^+ \rightarrow 0_1^+) = 100$.

I	$E_{s=1}$	$E_{s=2}$	B(E2)		B(E2) $I_2 \rightarrow J_1$		
			$I_1 \rightarrow (I-2)_1$	$I_2 \rightarrow (I-2)_2$	$J = I-2$	I	$I+2$
0	0	564.9					62.4
2	100	745.0	100	79.5	2.1	8.2	36.6
4	290.4	1068.9	159.9	120.0	0.9	6.1	27.9
6	543.0	1475.1	198.2	146.8	0.6	4.9	21.9
8	848.3	1944.1	227.6	169.3	0.6	4.1	17.6
10	1202.7	2468.7	250.9	188.6	0.5	3.5	14.6
12	1604.1	3045.4	269.7	205.1			

1.3.2 The exact numerical solution for the X(5) Hamiltonian: Caprio's solution

As mentioned the solution of the Bohr Hamiltonian under Iachello's approximation [2] gives the energy levels and the transition strengths which can be directly compared with the experimental results.

Recently, based on the numerical technique proposed by Rowe et al. [26], an exact solution of the X(5) Hamiltonian is proposed by M. A. Caprio [27].

Caprio solved the X(5) Bohr Hamiltonian without assuming separability. In the exact solution of the X(5) Hamiltonian levels are organized into defined bands characterized by strong intra-band transition strengths. The lowest energy bands have the spins contents associate to the gsb, β band and γ band. It results that the band head excitation energies, energy spacing within the bands, and the transition strengths are strongly dependent on the γ stiffness (it is valid for both γ and β bands). In Caprio's X(5) solution all the energy ratios and transition matrix elements obtained on the diagonalization of the Hamiltonian depend on the parameter a which measures the γ stiffness of the Hamiltonian. For $a = 0$, the potential is γ -independent, while for nonzero values of a yield confinement around $\gamma = 0$. Some of the spectroscopic features found in the approximate solution are encountered in the full solution (i.e. the larger energy spacing scale of the β band the yrast band¹ and strong interband E2 transitions are predicted), however some essential features of

¹ $E(2_\beta^+) - E(0_\beta^+) = 1.80E(2_1^+)$

the full solution are missing in the approximate solution: the dependence of the β band head energy on the γ stiffness, the confinement of the wave function near $\beta = 1$ due to the five-dimensional centrifugal effect and the consequent tendency of the energy and transition strengths observable toward rotational value for large γ stiffness. The staggering of the energies in the γ band are absent in the approximate solution. Detailed description can be found in [27]. It turns out that a value of $a \approx 200$ best agrees with the original X(5) prediction, indeed, for that case, the overlaps of the exact solutions with the approximate solutions are nearly unitary.

In figure 6.5 the schematic representation of the X(5) exact solution is shown.

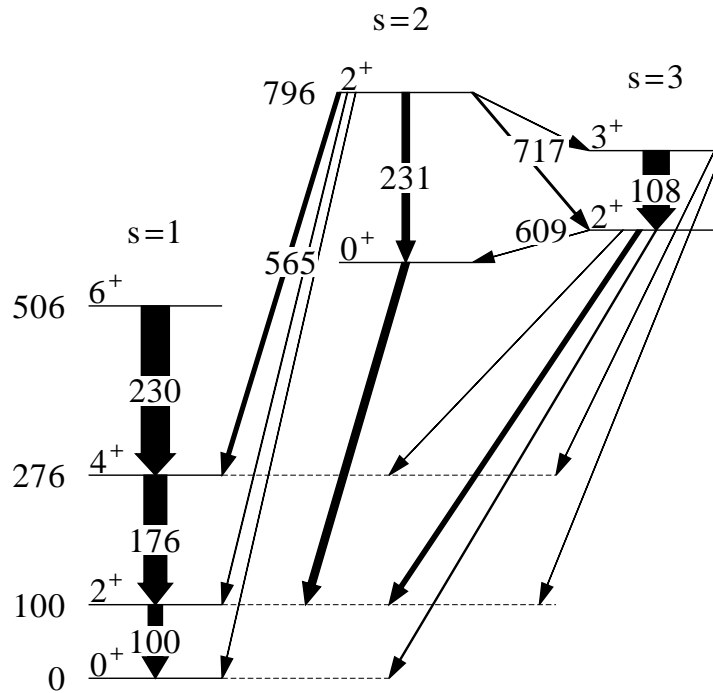


Figure 1.4: Schematic representation of the exact X(5) solution [27]. Energies are in units of the $E(2_1^+ \rightarrow 0_1^+) = 100$. The arrow thicknesses are full-scale adapted to the reduced transition probabilities.

In table 1.2 the energies of the exact X(5) solution for the gsb as well as for the β and γ bands are summarized.

In table 1.3 the predicted energies and transition probabilities for the

Table 1.2: Energies of the exact X(5) solution for the gsb as well as for the β and γ bands as reported in the tabulations [27, 28] for $a = 200$. Energies are in units of $E(2_1^+ \rightarrow 0_1^+) = 1$.

I	E_{S_1}	E_{S_2}	E_{S_3}
0	0.00	5.65	
2	1.00	7.96	6.09
3			7.17
4	2.76	11.04	8.11
5			9.50
6	5.06	14.66	10.58
7			12.31
8	7.79		

$s = 1$ band of the approximate and exact X(5) solution introduced in the previous sections are reported for comparison.

Table 1.3: Comparison of the predicted energies and transition probabilities for the $s = 1$ (gsb) band of the approximate [2] and exact X(5) solution. The energies and transition probabilities of the exact X(5) solution for the $s = 1$ are extracted from the tabulations [27, 28] for $a = 200$. Energies are in units of $E(2_1^+ \rightarrow 0_1^+) = 1$ and transition rates are reported fixing $B(E2; 2_1^+ \rightarrow 0_1^+) = 1$.

I	E_{approx}	E_{exact}	$B(E2)_{approx}$ $I \rightarrow (I - 2)$	$B(E2)_{exact}$ $I \rightarrow (I - 2)$
2	1.00	1.00	1.00	1.00
4	2.91	2.76	1.58	1.60
6	5.43	5.06	1.98	1.97
8	8.48	7.79	2.27	2.27
10	12.03	10.90	2.61	2.53

Chapter 2

Lifetime measurement in the picosecond region

The lifetime of an excited nuclear state can vary from 10^{15} years to 10^{-18} seconds. As an example, the radioactive decays of naturally occurring radioisotopes (e.g. ^{235}U , ^{238}U , ^{232}Th) have a half-life of 10^{15} y while the break up of highly unstable nuclei such as ^8Be and ^5He occurs with a lifetime in the range 10^{-16}s to 10^{-20}s . Several techniques have been developed to measure lifetimes. Each method allows to measure lifetimes in a specific time range. As an example, for lifetimes in the range of 10^{-3}s to 10^{-10}s the Delayed Coincidence technique is widely used. The Doppler shift Attenuation Method (DSAM) is applicable down to 10^{-14}s . For shorter time scales the Gamma Ray Induced Doppler broadening method (GRID) is used.

In this work lifetimes are expected to be in the range 10^{-9}s to 10^{-12}s . In this time range the Recoil Distance Doppler Shift (RDDS) method is widely used. The description of the technique is given in the next section.

2.1 The RDDS Method

The Recoil Distance Doppler Shift Method (RDDS)[29] is the standard in beam technique for measurement of lifetimes of excited states of nuclei in the picosecond region.

The experimental setup for the RDDS experiment consists of a chamber which contains two stretched foils (see fig.2.1) – the target and the stopper foils – mounted parallel to each other at a variable distance d . The scheme of the standard experimental setup is shown in figure 2.1.

Upon impact of the ion beam on the target nuclear reactions can be initiated. The typical reaction of interest here is the fusion evaporation

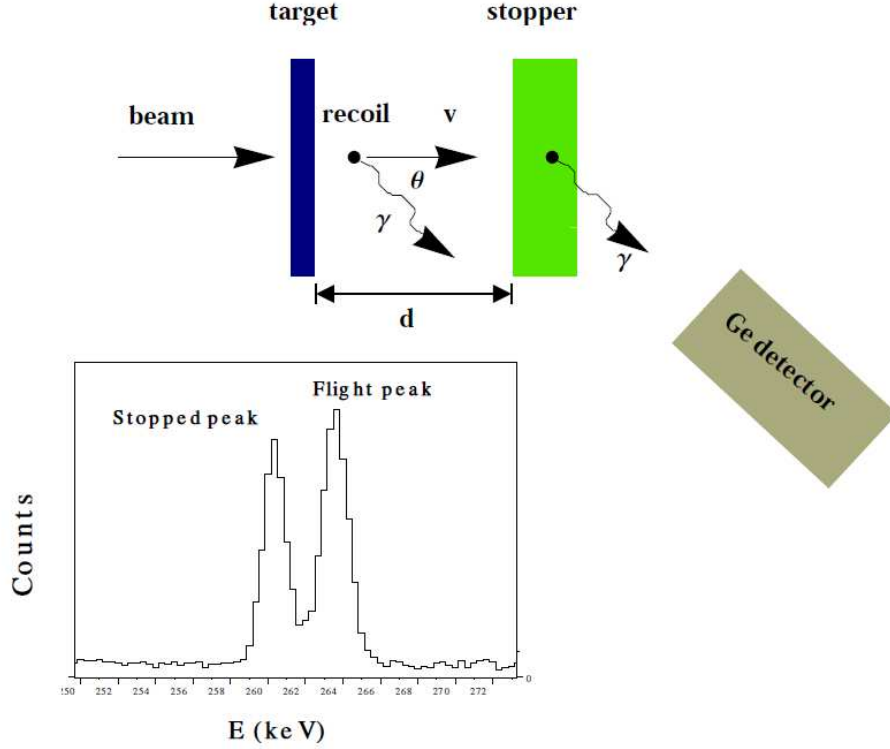


Figure 2.1: A schematic setup of an RDDS experiment.

reaction. The produced excited nucleus recoils with a velocity of few percent of the speed of the light in the direction of the stopper foil. After its creation the recoiling nucleus deexcites by the emission of a cascade of γ -rays which are registered by the surrounding detectors.

The recoiling nucleus, produced in an excited state, can deexcite by emission of γ -rays while it is in flight between the two foils or when it is at rest in the stopper foil.

In the second case, the registered energy E_γ is independent of the flight direction as the energy is not affected by Doppler broadening.

For the emission in flight the same transition will be observed with the Doppler shifted energy

$$E_\gamma^1 = E_\gamma \left(1 + \frac{v}{c} \cos \theta\right), \quad (2.1)$$

where E_γ is the energy of the unshifted component, E_γ^1 is the Doppler shifted component, θ is the angle with respect to the beam axis at which the γ -ray is observed, v/c is the recoil speed and c the speed of light in vacuum. The recoils, produced inside the target foil, are slowed down due to the interactions with the atoms¹ of the target foil. Nuclei which are created in the front part of the target foil are stronger decelerated than those which are created in the back part. A statistical distribution of the velocity with a mean value $\langle v \rangle$ of the recoil speed is then observed. Therefore in the γ spectrum for each transition two γ -ray peaks are present: one at the shifted energy and the second at the unshifted energy.

The intensities of the two components depend on the time of flight $t = d/v$ and on the lifetime of the level.

By changing the distance between the two foils the time of flight of the recoiling nuclei is changing and consequently the number of recoils which decay in flight or at rest will change accordingly. The lifetime is determined from the intensities of the two components. Of course in order to apply the method the effective lifetime² of the level of interest must be in the range of the RDDS Method. This depends on the recoil velocity and on the maximal distance set between the foils. The applicability of this method is typically limited to a time region from about 1ps up to 1000ps.

2.2 The Differential Decay Curve Method

The lifetime of a level is determined from its decay function which depends on the feeding times and the intensities of all the transitions which populate the level under examination. For a precise determination of the lifetime the complete feeding history is needed. In the conventional analysis of RDDS data all the observed decay curves are fitted by a set of coupled differential equations. The large number of parameters involved in describing the cascade potentially can complicate the analysis at this point. A transparent method of analysis of RDDS data has been proposed by A. Dewald [30], the so called Differential Decay Curve Method (DDCM). It allows for each level to replace the set of differential equations by a single first order differential equation of quantities obtained directly from the experimental data if all the direct feeders of the level of interest are known.

¹The process of slowing down of an ion in a solid is due mainly to the the inelastic collisions with the atomic electrons of the material and to the elastic scattering from nuclei. A detailed description of the processes can be found in [62].

²The effective lifetime describes the cumulative lifetime of a given level including all feeding times from cascades of levels above that level.

A full description of the method can be found in [30] and [31]. For completeness the model is briefly described below.

Figure 2.2 shows an arbitrary situation for a decay and feeding pattern of a level l_i of which the lifetime is to be determined.

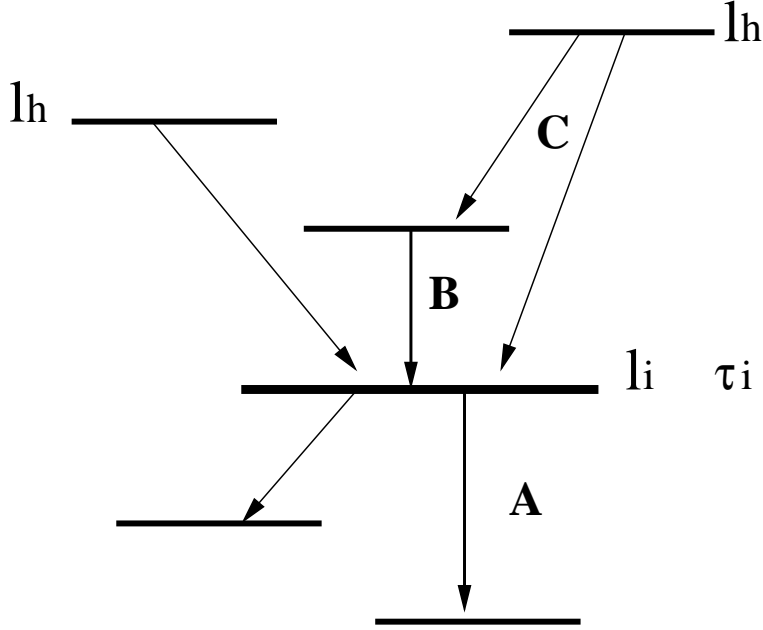


Figure 2.2: Arbitrary decay and feeding pattern of level l_i .

The level of interest l_i with lifetime τ_i is populated by several levels l_h .

Time evolution of the population $n_i(t)$ of the level l_i is given by the differential equation $\dot{n}_i = -\lambda_i n_i + \sum b_{hi} \lambda_h n_h$ where λ_i is the decay constant and \dot{n}_i is the number of decays per time unit.

In the pattern shown in figure 2.2 the level of interest is populated from other levels l_h , so the decay law becomes:

$$\dot{n}_i = -\lambda_i n_i + \sum_h b_{hi} \lambda_h n_h(t), \quad (2.2)$$

in which $n_h(t)$ is the number of nuclei in the level l_h at time t and λ_h is its decay constant; b_{hi} are the branching ratios of the decay of the level l_h to the level l_i .

Integrating the equation 2.2 and taking into account the relation $\lambda_i = \frac{1}{\tau_i}$ one obtains the basic relation for determination of the lifetimes:

$$\tau_i(t) = \frac{-N_i(t) + \sum_h b_{hi} N_h(t)}{\frac{dN_i(t)}{dt}}, \quad (2.3)$$

The quantities $N_i(t)$ and $N_h(t)$ are direct proportional to the shifted and unshifted peak observed in the RDDS experiment at distance $d = vt$ with t the time of flight of the recoils between target and stopper. The proportionality, for an experiment in singles mode, is related to the detector efficiency, the γ angular distribution, the conversion coefficients as well as the normalization factors (see paragraph 4.3). The lifetime, in a singles measurement, can be directly extracted from the spectra if all feeders are known.

For each $t_i = d_i/v$, given by a distance d_i between target and stopper, an independent lifetime τ_i of the level of interest is extracted. The plot of the τ_i versus d is called τ -plot or τ -curve. Each deviation of the τ -curve from an horizontal line indicates clearly the presence of systematic errors in the measurement or in the extraction of the lifetime. There is a range of distances, called *sensitive region*, in which the obtained lifetimes exhibit a comparably small statistical error.

Typical systematic errors are related to wrong assumptions on intensities of feeding transition, unobserved feeding, contaminations and deorientation effect³.

2.2.1 The DDCM for coincidence measurements

Many of the problems caused by systematic errors in the analysis of singles RDDS experiments can be avoided in coincidence experiments [30, 31]. The feeding pattern can be simplified by gating only on one feeding transition and problems like the unobserved feeding which can create errors in the extraction of lifetimes are bypassed.

The measured intensities of two transitions in coincidence X and Y, where transition Y occurs first, are indicated $\{Y, X\}$. Using the label (S) and (U) respectively for the shifted and unshifted components of a transition in an RDDS coincidence experiment, the coincidence intensities Y, X can be written as:

$$\{Y, X\} = \{Y_U, X_U\} + \{Y_S, X_U\} + \{Y_S, X_S\} + \{Y_U, X_S\}, \quad (2.4)$$

where $\{Y_U, X_S\} = 0$ because a nucleus stopped after the transition Y_U can not decay in flight afterwards.

³The deorientation effect observed in nuclei recoiling into vacuum is due to the hyperfine interactions between the spins of the atomic nucleus and the surrounding electron configuration with a consequent rearrangement of the distribution of the emitted radiation. For details see [32, 33].

The formula 2.3, valid for singles measurements can be written in the coincidence formalism as:

$$\tau(t_k) = \frac{\{C_S, A_U\}(t_k) + \alpha\{C_S, B_U\}(t_k)}{\frac{d\{C_S, A_S\}(t_k)}{dt}}, \quad (2.5)$$

where $t_k = \frac{d_k}{v}$ and α is the branching ratio of the intensities $\{C, A\}$ and $\{C, B\}$

$$\alpha = \frac{\{C, A\}}{\{C, B\}} = \frac{\{C_U, A\}}{\{C_U, B\}} = \frac{\{C_S, A\}}{\{C_S, B\}} = \frac{\{C_S, A_U\} + \{C_S, A_S\}}{\{C_U, B_U\} + \{C_U, B_S\}}, \quad (2.6)$$

A simplification of 2.6 is obtained if the energy gate is set on the direct feeder B of the level l_i . Indeed with this condition the equation 2.5 becomes:

$$\tau(t_k) = \frac{\{B_S, A_U\}(t_k)}{\frac{d\{B_S, A_S\}(t_k)}{dt}}, \quad (2.7)$$

Some major advantages of the DDCM analysis for coincidence measurements are pointed out in the following:

- Only directly observed feeding transitions are used to determine the lifetime. By setting the coincidence conditions the problem of the unknown feeding is bypassed.
- Only relative target-to-stopper distances are used for the analysis. There is no need to determine absolute distances (valid also for singles measurements).
- The effect of the angular correlation and the Deorientation effect on the low-lying states are bypassed [32] when the gate is set on the shifted component of a direct feeding transition.

Chapter 3

Experimental details

Three **R**ecoil **D**istance **D**oppler **S**hift experiments have been performed with the Köln coincidence plunger device to extend the experimental information on the lifetimes of low-lying excited states of the $^{176,178}\text{Os}$ nuclei.

The first RDDS experiment for the measurement of lifetimes in ^{176}Os was performed with the coincidence plunger device mounted at the GASP spectrometer of the Laboratori Nazionali di Legnaro (Italy). The beam was provided by the XT Tandem accelerator of the laboratory. The aim of this first experiment was to determine the lifetimes of the ground state band levels in ^{176}Os .

The second and third experiment with the coincidence plunger device were performed at the FN Tandem facility at the Institute für Kernphysik of the University of Cologne.

These last two experiments were devoted to remeasure the lifetimes of the first excited states in $^{176,178}\text{Os}$ with RDDS technique. O. Möller et al [3] measured for the first time the lifetimes of the first excited 2^+ in $^{176,178,180}\text{Os}$ using the delayed coincidence technique.

In this chapter details about the experimental setups are reported.

3.1 The Plunger device

For the RDDS experiments described in this work the Köln plunger device was used. This device has been built at the Institute of Nuclear Physics of the University of Cologne, Germany. The picture in figure 3.1 shows a drawing of a section of the Cologne plunger apparatus. In the figure 3.1 one can clearly distinguish the reaction chamber (on the left with a ball shape), the stopper foil is fixed in the center of the chamber while the target mounting plate is located on the left end of the beam-tube (center, in blue). The motor is

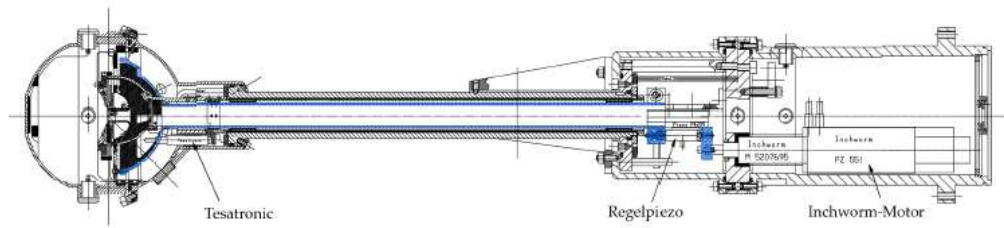


Figure 3.1: Drawing of the Cologne plunger apparatus [30].

located at the right end of the apparatus. With this system and the related electronics it is possible to set distances between the target and stopper from electrical contact to about $2000 \mu\text{m}$ with an accuracy of $0.5 \mu\text{m}$. The foils are glued on special aluminum rings mounted and stretched on aluminum cones. It is essential that the foils are flat and stretched so that they can be positioned at very short distances to each other and remain flat during the heavy-ion beam bombardment. In figure 3.2 a gold stopper foil is shown, glued on the ring and mounted on the cone. The foil is stretched and ready to be mounted in the plunger chamber.



Figure 3.2: A gold stopper foil is mounted and stretched on the aluminum cone.

The two foils in the plunger chamber are mounted parallel to each other and perpendicular to the beam direction. Modification of the distance between the foils is done by changing the target position with a linear motor

called *Inchworm*. The motor consists of three piezo-crystals and also incorporates its own optical measurement system for the position determination. The *Inchworm* allows to set relative distances between the foils with a precision of $0,5 \mu\text{m}$. The target is connected to the linear motor through a connection tube mounted concentric inside the beam-tube (see figure 3.1). Additionally, an independent inductive distance transducer – a Tesa-probe (TESATRONIC)– is mounted inside the target chamber. The inductive system, and also the optical Inchworm, can only measure relative distances from the mechanical structure of the fixed stopper and the target. A measurement of the target-to-stopper distance is performed by measuring the capacitance of the parallel-plate capacitor formed by the target-to-stopper system [49]. Before the start of each measurement, with a cold plunger, the capacity versus the distance, is measured with the Tesa-probe (see paragraph 4.2). As the beam arrives on the foils the energy loss of the ion beam in the foils induces a thermal expansion of all the parts of the target and stopper system. Of course, for the high precision required for this kind of experiment these variations cannot be neglected. On the other hand, these expansions are not in equilibrium. The beam current typically does not stay constant enough to keep the temperature constant of the mechanical structure. It is therefore necessary to compensate for the resulting changes of the target-to-stopper distance by a feedback mechanism. Between the Inchworm and the connection tube another piezocrystal is mounted. With this piezocrystal a change of the distance between the foils caused by a change of the beam conditions can be automatically balanced with a change of the distances between the foils (the regulation is up to $30 \mu\text{m}$). As above mentioned, the isolated target-to-stopper system forms a parallel-plate condenser and the dependence of capacity from the distance of the foils is used as basic signal for the feedback system. An electric pulse is applied to the target foil to measure the capacity between target and stopper foil. The signal of the stopper is amplified and converted by the ADC (Analog–Digital–Converter) and controlled by a PC. If the capacity exceeds outside the range with prescribed tolerance, the feedback system will automatically compensate this by changing the distance between the foils.

3.2 The GASP spectrometer

The GASP 4π spectrometer has been developed and built at the Laboratori Nazionali di Legnaro (LNL), Italy [34]. It consists of 40 large-volume high purity Germanium detectors (HPGe), each with a relative efficiency of about 82%. The total solid angle covered by the HPGe detectors is 10%.

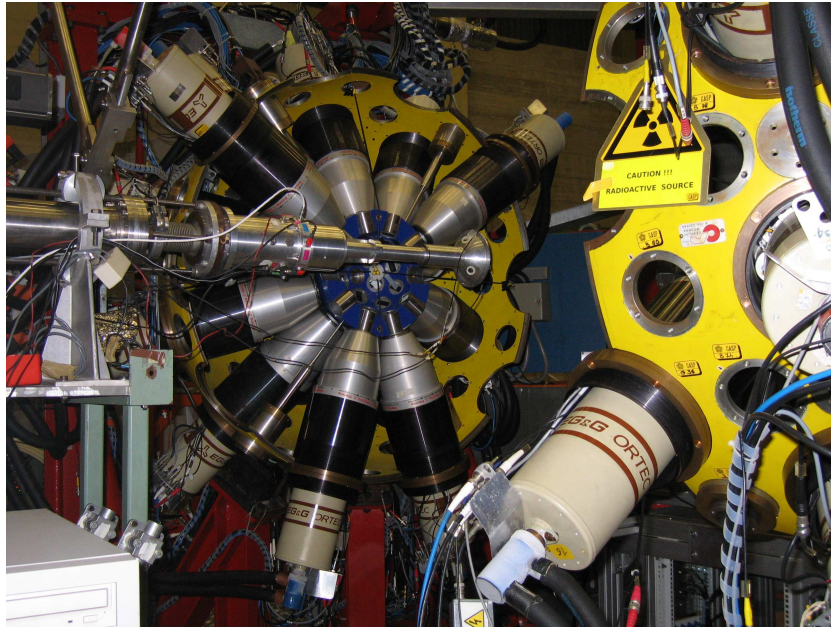


Figure 3.3: The GASP spectrometer in open condition and for configuration C1. The picture shows the Cologne Plunger device as it is mounted in the spectrometer.

The 40 HPGe detectors of GASP can be grouped in 7 rings. The detectors within each ring are positioned under almost identical angles with respect to the beam axis. The detectors are divided in two hemispheres (see fig.3.3). Table 3.1 summarizes the distribution of the 40 detectors over the 7 rings. In the standard configuration I (C1) the 40 detectors are placed at 27cm from the target position and mounted in a BGO Compton-suppression shield. For this configuration the total absolute photo peak efficiency is 3% at a gamma-ray energy of 1332 keV. In addition it provides a 4π BGO multiplicity filter (called BGO Inner Ball) which consists of 80 individual BGO crystals acting as active collimator and measuring the total energy and the multiplicity of the gamma cascades.

In the configuration II (C2) the BGO Inner Ball is removed, the collimator function is obtained by a Pb shield of similar geometry as the BGO Inner Ball but with a smaller diameter. This shield has been made in collaboration with the Institute für Kernphysik of the University of Cologne, Germany. In this configuration the HPGe detectors are mounted at a shorter distance from the target position (20 cm) with a corresponding increase of the total photo peak efficiency to 5.8%. The plunger device has been coupled with the

GASP spectrometer in configuration II for the experiment discussed in this work.

Table 3.1: Distribution of the 40 HPGe detectors of GASP over 7 rings.

Ring number	Angle [°]	Number of Detectors
0	34.6	6
1	59.4	6
2	72.0	4
3	90.0	8
4	108.0	4
5	120.6	6
6	145.4	6

3.3 The ^{176}Os experiment at GASP

In this paragraph details on the coincidence recoil distance experiment performed at the Laboratori Nazionali di Legnaro for measuring lifetimes in ^{176}Os are reported.

Excited states of ^{176}Os were populated via the reaction $^{152}\text{Sm}(^{29}\text{Si},5n)^{176}\text{Os}$ at a beam energy of 158 MeV. The beam was provided by the XT tandem accelerator of the Laboratori Nazionali di Legnaro, Italy. The coincidence plunger apparatus of the University of Cologne was mounted in the GASP spectrometer in configuration II. For this experiment the GASP detectors located at the same polar angle θ with respect to the beam axis were grouped into rings. That way the spectrometer was subdivided into 7 different rings (see table 3.1). The target consisted of 0.5 mg/cm^2 ^{152}Sm evaporated onto a 1.98 mg/cm^2 Ta foil backing. A 7.7 mg/cm^2 gold foil was used to stop the ^{176}Os recoil nuclei which left the target with a mean velocity of 1.53(2)% of the speed of light.

Table 3.2 summarizes all the details for the experiment at GASP.

The CASCADE calculation code [35] was used in preparation of the experiment. (The predicted cross sections as function of beam energy are shown in Fig.A.1 in appendix A). An optimal beam energy was estimated (at 150MeV) corresponding to the maximum in the cross section. A thin layer of ^{181}Ta was chosen as backing material for the target. The energy loss

Table 3.2: Technical details of the plunger experiment at GASP.

Experiment	^{176}Os
Reaction	$^{152}\text{Sm}(^{29}\text{Si},5\text{n})^{176}\text{Os}$
Beam energy	$E(^{29}\text{Si}) = 158 \text{ MeV}$
Beam current	$I(\text{Cup}) = 2 \text{ pA}$
Charge status	$C(^{29}\text{Si}) = 10^+$
Target	0.5 mg/cm^2 of ^{152}Sm
Backing	1.98 mg/cm^2 of ^{181}Ta
Stopper	7.7 mg/cm^2 Au
Recoil velocity	$v/c = 1.53(2)\%$
Distances [μm]	3.53;5.50;7.44;10.86;15.26; 21.15;26.01;33.83;46.3;59.24; 78.76;108.11;147.20;196.1; 254.7;376.9;660;1000

in the target by the beam was calculated to be $E_{loss} \sim 8\text{MeV}$, as calculated with VTL [36]. To account for this energy loss, the requested beam energy was increased with this amount. Factors which must be taken in consideration while fixing the beam intensity are: the Ge mean single rate which must not exceed 10kHz (too high singles rate will spoil the resolution) and the heat induced by the beam on the target. As reported in the work [37] the beam current must be kept below the current that can induce deformation in the target or stopper foils.

With the VTL program, developed at IKP of the University of Cologne, it is possible to extract the maximum beam current without inducing deformations (bumps) in the foils. For this experiment the beam current of 2 pA was chosen.

It is necessary to take in consideration that also the thickness of the target plays a significant role. A thicker target may yield more reaction products of interest. On the other side, it also makes larger straggling of the secondary reaction products, which cause larger Doppler broadening of the in-flight components. On the basis of these considerations, for this measurement was used a target thickness which results from a compromise between a higher statistic and a lower energy resolution.

Evidently, the thickness of the stopper foil must be chosen such that the recoils are stopped. However, choosing the stopper foil too thick might cause an increase of background due to the Coulomb excitation of the stopper

material by the primary beam. The stopper material should be chosen such that the produced background lines do not overlap with the lines in the spectrum of the nucleus of interest. In this experiment a gold foil was used. The γ rays deexciting the ^{176}Os , produced in the dominant reaction channel, were registered with the GASP spectrometer. $\gamma\gamma$ -coincidences were taken at 18 different target-to-stopper distances from the electrical contact point of the target and stopper foil up to $1000\ \mu\text{m}$ separation. The separations used are listed in table 3.2. At the end of the measurement a calibration with a ^{152}Eu source was done. The source was positioned in the plunger at the stopper position which corresponds to the center of the GASP spectrometer. In this experiment lifetimes of levels in the ground state band (gsb) were measured and in two excited bands with negative parity. The β and γ -bands were not populated. In figure 3.4 spectra of transitions of ^{176}Os measured at distances of 5, 25 and $150\ \mu\text{m}$ with the detectors positioned at 34.6° with respect to the beam axis are shown. In the spectra three transitions of the gsb which show the effect of the Doppler broadening are indicated with labels (U stands for unshifted component and S for shifted component). Lifetimes in the neighbor $3n$ reaction channel ^{177}Os could be extracted, too.

3.4 The $^{176,178}\text{Os}$ experiments at the Cologne FN Tandem accelerator

In this paragraph details of the two coincidence recoil distance Doppler-shift experiments performed at the FAN Tandem of the University of Cologne are reported.

Excited states in ^{178}Os and ^{176}Os were populated via the reaction $^{164,166}\text{Er}(^{16}\text{O},4n)^{176,178}\text{Os}$ at the primary beam energies of 86 MeV and 80 MeV, respectively. The experimental setup for both experiments consisted of one Euroball cluster detector containing 7 encapsulated HPGe detectors, five single large volume HPGe detectors and one planar HPGe detector. The central Euroball cluster detector was positioned at 0° while the other six crystals span a complete ring with an angle of 30° with respect to the beam axis. The five large volume HPGe detectors were positioned at 143° and the planar HPGe detector at 0° , positioned between the plunger head-cup and the Euroball cluster. The purpose for using the planar detector¹ is its high energy resolution for low energy transitions, because of the small capacity of the detector. This was essential in these two RDDS experiments since

¹The planar detector used is an HPGe detector with a volume of 22cm^3 and energy resolution of 750 eV at 122 keV

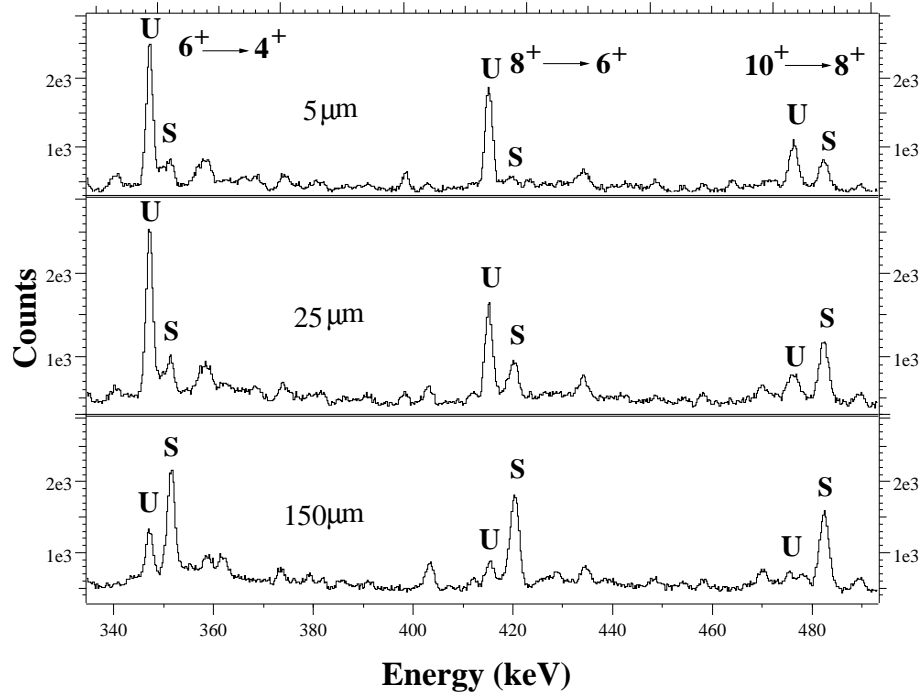


Figure 3.4: Spectra of transitions of ^{176}Os measured at distances of 5, 25 and $150\ \mu\text{m}$ with the detectors positioned at 34.6° with respect to the beam axis. The components of transitions in the gsb of ^{176}O which show the effect of the Doppler broadening are indicated with labels. The label U stands for the unshifted component and S for the shifted component.

the aim was to measure lifetimes of the first 2^+ excited states in $^{176,178}\text{Os}$ with energy of 132.4 keV and 135.1 keV, respectively. The Cologne plunger apparatus was used in combination with these detectors. Details of the two experiments are reported in table 3.3 and described in the following sections.

The first RDDS experiment was performed to measure the lifetime of the first excited 2^+ state in ^{178}Os .

A self-supporting target of $0.5\ \text{mg}/\text{cm}^2$ of ^{166}Er and a gold stopper foil of $3.6\ \text{mg}/\text{cm}^2$ of thickness have been mounted in the plunger chamber. $\gamma\gamma$ -coincidences were taken at 7 distances from the electrical contact between target and stopper up to $4000\ \mu\text{m}$. Figure 3.4 shows the spectra where the effect of the lifetime is evident. The resulting lifetime is also compared to the measured value obtained using the Delayed Coincidence Method [3].

The second RDDS experiment at the FAN Tandem accelerator has been performed to measure the lifetime of the 2^+ state in the ground state band

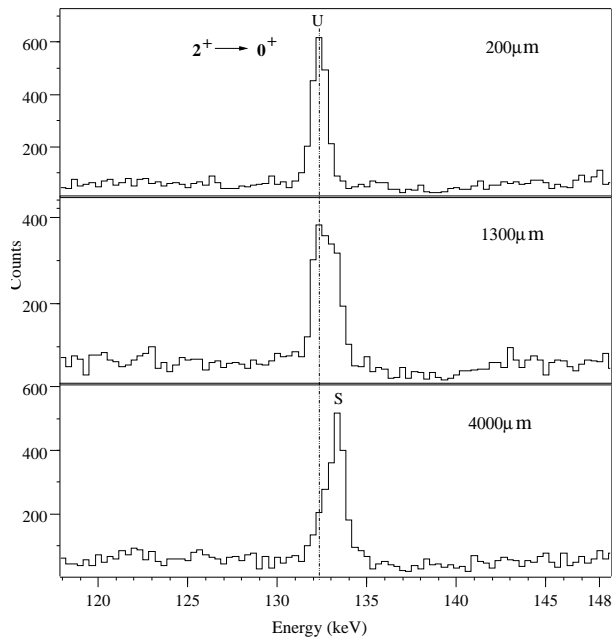


Figure 3.5: Spectra of ^{178}Os measured at distances of 200, 1300 and 4000 μm between the foils with the detector at 0 deg with respect to the beam axis. The two components of the $2_1^+ \rightarrow 0_1^+$ transition are indicated. The label U stands for the unshifted component and S for the shifted component.

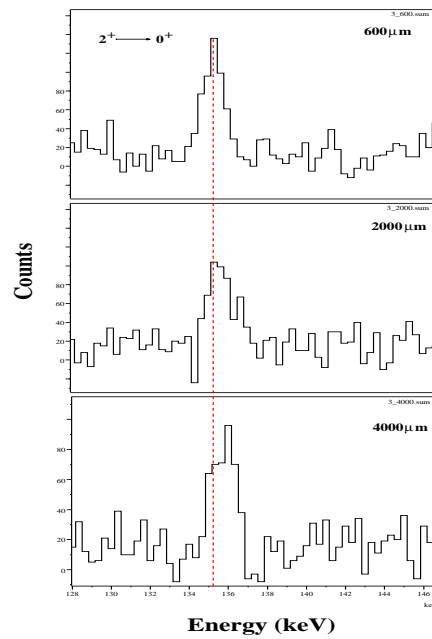


Figure 3.6: Spectra of ^{176}Os measured at distances of 600, 2000 and 4000 μm between the foils with the detector at 0 deg with respect to the beam axis. The two components of the $2_1^+ \rightarrow 0_1^+$ transition are indicated. The label U stands for the unshifted component and S for the shifted component.

Table 3.3: Technical details of the experiments at the FAN tandem, Cologne.

Experiment	^{176}Os	^{178}Os
Reaction	$^{164}\text{Er}(^{16}\text{O},4\text{n})^{176}\text{Os}$	$^{166}\text{Er}(^{16}\text{O},5\text{n})^{178}\text{Os}$
Beam energy	$E(^{16}\text{O}) = 86 \text{ MeV}$	$E(^{16}\text{O}) = 80 \text{ MeV}$
Beam current	$I(\text{Cup}) = 2 \text{ pA}$	$I(\text{Cup}) = 2 \text{ pA}$
Charge status	$C(^{16}\text{O}) = 8^+$	$C(^{16}\text{O}) = 8^+$
Target	0.9 mg/cm^2 of ^{164}Er	0.5 mg/cm^2 of ^{166}Er
Backing	1.6 mg/cm^2 of ^{181}Ta	NO
Stopper	3.5 mg/cm^2 Au	3.6 mg/cm^2 Au
Recoil velocity	$v/c = 0.52(2)\%$	$v/c = 0.70(2)\%$
Distances [μm]	16.0;600;1213;1619; 2013;2924;4023;6033;	3.01;200;191.8;592; 1292;2192;3992;

of ^{176}Os .

A 62.4% enriched ^{164}Er (24.3% ^{166}Er) target of thickness 0.7 mg/cm^2 evaporated on to 1.6 mg/cm^2 of ^{181}Ta was used for this measurement. $\gamma\gamma$ -coincidences were taken at 8 distances between target and stopper from the electrical contact up to $6000 \mu\text{m}$. At the end of each experiment an energy calibration was done with an ^{152}Eu source mounted at the stopper position. Figure 3.6 shows the spectra where the effect of the lifetime is evident.

Chapter 4

Data analysis

This chapter describes step by step all the procedures used to estimate lifetimes of the levels of interest starting from the raw data.

The calibration, the shift-correction, the sort of the data in matrices, the determination of the distances, the normalization, the determination of the intensities in the gated spectra and analysis of the lifetime with the DDCM are reported in this chapter in detail.

The procedures described here have been applied to all three experiments discussed in this work.

4.1 Calibration and Shift-correction

At the end of each experiment the energy calibration for each detector is required. In this way a correspondence between energy and channel for each detector is defined. For all the experiments the ^{152}Eu source has been used. The instability of the (front-end) electronics can introduce a gain shift in the spectra during the measurement. This means that the calibration for one detector can change over time. The correction of this gain-shift, the recalibration of the spectra, ensures that all detectors will have identical gains for the data taken during the entire measurement. To make this correction the acquired data was stored in runs of one hour each. In this way, it is easy to follow the possible fluctuations of the γ -lines for each detector and use them as reference in the successive runs.

The coefficients used to perform the correction are determined from projection spectra produced by a pre-sort. These projections are produced for each run. One of the runs is taken as reference for the others. Two γ -lines, unaffected by Doppler broadening, are used for comparison within the same detectors for all runs. This procedure is applied to each detector.

The time spectra (i.e. time difference spectra giving the time between the individual detector signal and the coincidence trigger signal) are not strongly affected by electronic instabilities¹, and only the spectra of the individual detectors for any arbitrary run had to be shifted on top of each other by addition of a constant time (–value). With the times of the detectors shifted this way, the time difference spectra for each detector combination were sorted, in which the time distance between two coincident events were incremented. In the time difference spectra two time windows are selected. The first one of about 40 ns is centered on the prompt peak and the second one is used for the background correction². Using this information for sorting the final coincidence matrices two kind of matrices are created. One with the events of interest and the second one with the background. The 4kx4k coincidence matrices $M_{M,N}^d$ are sorted for each distance d and for each combination of rings N and M.

4.2 Distance calibration

At the beginning of each plunger experiment, the capacity of the target-stopper foils system is measured against the distance given by the micrometer (Tesa) device. This measurement is done with the cold plunger, without beam and without an active feedback system.

What is stored is the voltage³ at each measured distances. The data are interpolated with a second order polynome over separate intervals. In fig. 4.1 the distance calibration is shown for the measurement done in LNL. With this calibration the voltage values of the system, kept constant by the regulating system, can be recalculated into relative distances during the measurement. At short distances the target-stopper system behaves electrically as a parallel plate capacitor (with a capacity C given by $C \propto \frac{1}{d}$ where d is the distance between the plates/foils) and has therefore a linear calibration curve (see fig. 4.2).

¹The timing is dependent on the sharp rise-time of the germanium detector signals and small changes in amplitude over time do not change timing performance.

²In this case the window consists of two selected intervals, one on the left and the other on the right of the window on the prompt peak.

³Actually what is measured is not the voltage between the foils but the induced charge proportional to the impulse amplitude as described in [49] where the capacity is related to the voltage by $C = \frac{Q}{V}$ with Q charge that may be stored for a given voltage V between the plates.

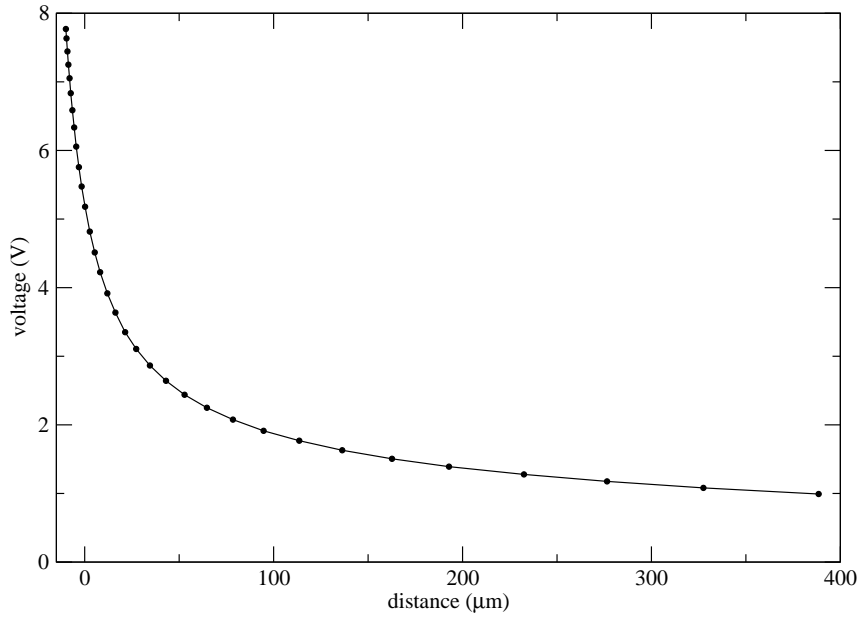


Figure 4.1: Distance calibration of the RDDS for the ^{176}Os experiment.

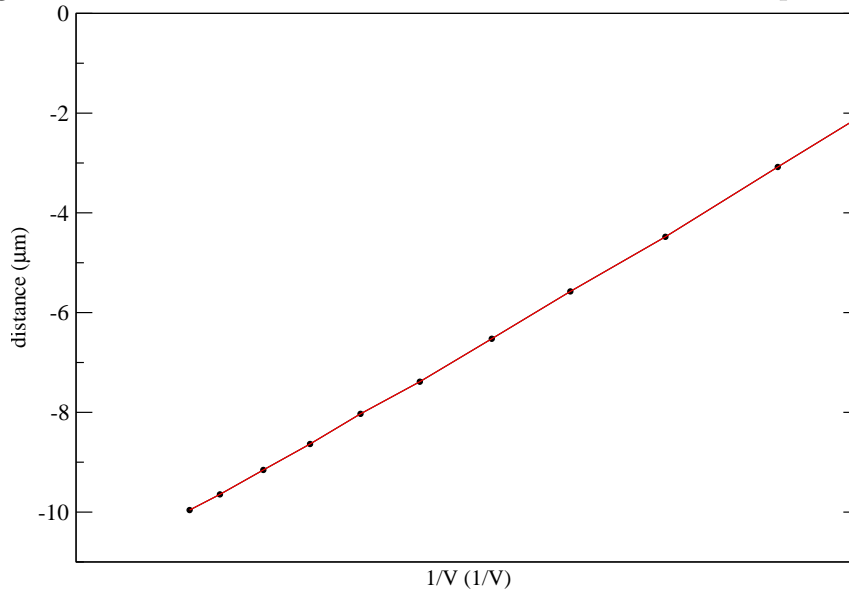


Figure 4.2: Capacity of the system target-to-stopper at short distances.

4.3 Normalization

Since information must be compared at each distance set between the target and stopper in order to extract the lifetime of the level, it is necessary that they refer to the same number of recoils produced in the reaction. The number of the recoils produced is related to the beam intensity.

The intensities of the shifted and unshifted components have to be corrected for differences in running time and beam intensity for different distances and normalized to the total number of reactions per distance.

The common normalization factors $N(d)$ for each distance d were determined from the total number of coincidences in strong cascades in a strong reaction channel. The intensities of the transitions used to determine the normalization factors have been taken from gated spectra where the gate is put on the unshifted and shifted component of one of the low-lying states of the ground state band.

In particular, the normalization factors for the experiment performed at LNL are obtained from the intensities of the sum of the flight and stopped components of transitions in the gsb of ^{176}Os in spectra created by gating on low-lying transitions $4^+ \rightarrow 2^+$, $6^+ \rightarrow 4^+$ and $8^+ \rightarrow 6^+$. The gate on the transition $2^+ \rightarrow 0^+$ was not taken into account because it could be affected by deorientation effects (see paragraph 2.2 and reference [41]). As example in table 4.1 the normalization factors are shown obtained for the ^{176}Os measurement.

Table 4.1: Normalization factors $N(d)$ for the ^{176}Os measurement at LNL. These values are valid for all the GASP rings used in the analysis.

Distance [μm]	$N(d)$	Distance [μm]	$N(d)$
3.53	1.174 (5)	59.24	1.333 (6)
5.50	1.093 (4)	78.76	1.356 (6)
7.44	1.000 (3)	108.11	1.414 (6)
10.86	1.113 (4)	147.20	1.402 (6)
15.26	1.151 (5)	196.1	1.404 (6)
20.15	1.228 (5)	254.7	1.424 (6)
26.01	1.133 (5)	376.9	1.604 (7)
33.83	1.243 (5)	660	1.887 (9)
43.6	1.274 (5)	1000	2.03 (1)

4.4 The recoil velocity

The recoil velocity is determined by the position of the shifted and unshifted components of the transition affected by the Doppler effect. The velocity v of the recoil nucleus, relative to the speed of light c , is deduced by the formula:

$$E_{\gamma}^1 = E_{\gamma}^0 \left(1 + \frac{v}{c} \cos \theta\right) \quad (4.1)$$

where E_{γ}^0 is the energy of the unshifted component and E_{γ}^1 is the Doppler shifted component.

The recoil velocity is extracted from the energy position of the two components from gated spectra at several detector rings. The information from the backward ring can be used as check for the value obtained for the ring around 0° .

In the analysis of the GASP experiment only those rings have been included where the Doppler effect is relevant (ring 0, 1, 5 and 6).

Gated spectra at short and large distances are used to get the position of the unshifted and shifted components, respectively. For the experiment performed at LNL, the position of the two components for the $4^+ \rightarrow 2^+$, $6^+ \rightarrow 4^+$ and $8^+ \rightarrow 6^+$ transitions of the recoil nucleus have been used for this purpose. The measured velocity in percent of the speed of the light is 1.52(2)%.

4.5 Application of the DDCM and the extraction of the lifetime

In the framework of the DDCM the mean lifetime of the level of interest is extracted directly from the observed coincidence intensities for each target-to-stopper distance. In an ideal case a coincidence condition can be set on the flight component of the direct feeding transition of the level of interest (direct gate). In case of presence of contamination of this component by an other line, the coincidence condition must be set on the shifted component of an indirect feeding transition (indirect gate). For each ring combination and for each target-to-stopper distance a coincidence spectrum is produced in which the intensities of the in-flight and stopped components of the transition which depopulates the level of interest are then determined (direct gate). In the indirect gated spectra the intensities of the transition which depopulates the level of interest and the components of the transition which populates that level must be determined. Special care must be taken at that

phase of the analysis to avoid a possible contamination spoiling the lifetime determination.

The coincidence window (gate) must be chosen in such way that no contaminations are contained. A possible contamination of the line is a transition which indirectly feeds the level and as such it contributes to the intensity of the line under examination. Since in the frame of the DDCM the lifetime of the level is extracted from the observed coincidence intensities it is necessary to pay attention to contaminations.

The background energy gate window must be chosen in such way that the background in the region of the line of interest is well represented and the produced background spectrum, which is subtracted from the coincidence spectrum, should not contain lines which spoil the analysis of the line intensity. The choice the background window were made indispensably test with different coincidence windows.

It seems to be more efficient to take in advance precautions to avoid possible contaminations, like the use of smaller coincidence windows and to renounce to some of the possible combination of rings than to make additional corrections to the measured intensities.

In fig. 3.4 an example is shown from the experiment performed at LNL. The two components of the line which are Doppler shifted are marked. This effect pronounces differently for different target-to-stopper distances.

The intensities of the shifted and unshifted peaks have been determined, where it was possible, by integration. In special ring combinations or in presence of a contamination, a Gauss curve was fitted to the lines. For the determination of the intensities of the lines by fitting, the parameters of the fit, the peaks positions and their widths were fixed while the peak area was a free parameter. For the determination of the width (fwhm⁴) of the peaks⁵ width calibrations were done.

4.5.1 The lifetime τ

The determination of the lifetime by the equation 2.5 or 2.7 is obtained by the program Napatau [38]. The intensities of the lines contained in the input file of the program are normalized (see paragraph 4.3) by the program which fits the intensity of the flight peak and calculates over separate intervals the derivative of that curve. The trend of the time-derivative is then adapted to the trend of the stopped peak intensities. For each target-to-stopper distance

⁴full width half maximum

⁵The fwhm of a peak result to be [39] proportional to the square root of the transition energy.

a lifetime τ is calculated. The value of the lifetime at each distance which lies in the sensitive region are displayed by the graphical output of Napatau. This plot is called τ -plot or τ -curve. The τ -curve is expected to be constant. Each deviation from an horizontal line indicates clearly the presence of systematic errors in the measurement or in the extraction of the lifetime. As an example of the graphical results given by Napatau two τ -plots are shown in fig. 4.3 and 4.4. The determined lifetime, calculated as average of the single values, is also indicated with its uncertainties.

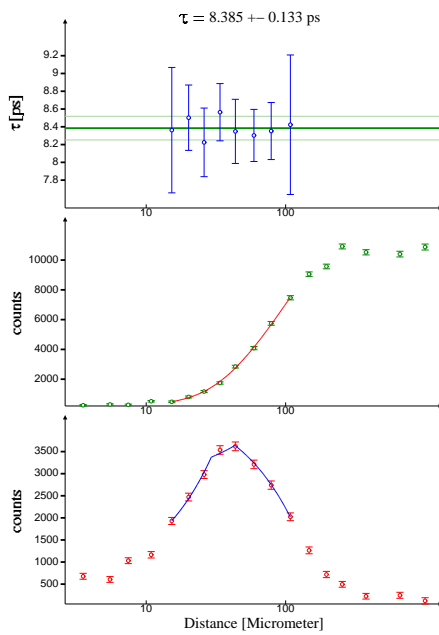


Figure 4.3: Napatau graphical representation: Lifetime of the 6^+ in ^{176}Os . From the top to the bottom respectively: τ curve, the shifted intensity I_{sh} and in the last plot I_{un} is fitted simultaneously with the derivative $\tau \frac{dI_{sh}}{dx}$.

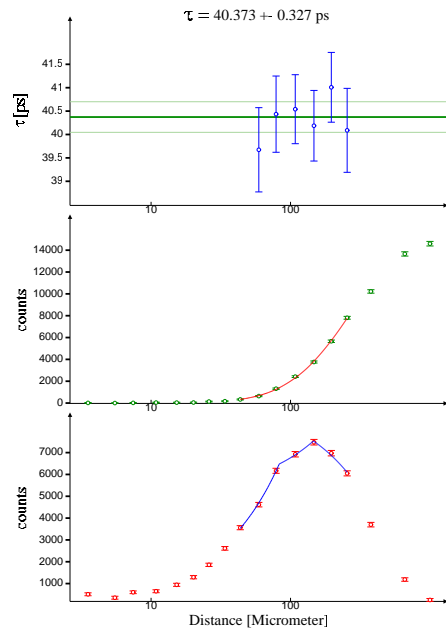


Figure 4.4: Napatau graphical representation: Lifetime of the 4^+ in ^{176}Os .

Chapter 5

Experimental results

In this chapter the experimental results are reported which were obtained from the RDDS experiments described in the previous chapter. A full description of the determination of each single lifetime measured in these experiments is given, specifying the uniqueness of each case. In the previous chapter, two different ways of producing gated spectra have been mentioned: the direct method and the indirect method. In this work the direct gate technique has been used mostly. The indirect gate method has been used as check in some cases and where the direct gating was not possible due to the presence of contaminating transitions. For each level of interest, gated spectra for each detector ring have been created. The direct gate method has been preferred because it gives results which are not influenced by the hyperfine interactions (deorientation effect) when the gate is set on the shifted component of the direct feeder [32]. The gate window has been set on the shifted component of the feeding transition of the state under investigation and the intensities of the in-flight and stopped peak components of the depopulating transitions have been determined.

Where it was possible, the intensities of the shifted and unshifted peaks have been determined by integration but in special ring combinations or in presence of a contaminant peak, a Gaussian curve was fitted to the lines. In the second case the positions and the width of the in-flight and stopped peaks have been fixed. For both the components the line-width versus the energy has been determined and used in the fit procedure. The software TV was used for analyzing the spectra [38].

5.1 The experiment at GASP: ^{176}Os

In total the lifetimes of 10 states in the ground state band and in two excited bands have been determined in ^{176}Os . For the determination of these lifetimes only the rings of GASP where the Doppler shift effect is relevant have been taken into account. It means that only the rings 0, 1 at forward angles and 5, 6 at backward angles have been used (see paragraph 3.2). Analyzing the spectra of these rings a maximum of 4 lifetime values were determined for every state. The lifetimes obtained from different $\gamma\gamma$ coincidence matrices as well from different gates are statistically independent and can be used to check the results for consistency. The final value of the lifetime τ of every level of interest was derived by averaging the individual results.

The ring at approximately 90° (ring 3) has been used to check for contaminations and to identify lines from other reaction channels.

In fig. 5.3 a partial level scheme of the nucleus ^{176}Os is shown [40].

5.1.1 Analysis of the ground state band

Lifetimes of states with spin 4^+ up to 12^+ in the ground state band (gsb) were measured.

- Spectra for the analysis of the 4^+ level in the gsb have been created by a gate on the $6^+ \xrightarrow{347\text{ keV}} 4^+$ direct feeding transition. All the relevant rings can be used to determine the lifetime of the 395 keV state since no contaminants are present.
- The direct gate method was used also to extract the lifetime of the 6^+ state. Gated spectra produced by gating on the shifted component of the $8^+ \xrightarrow{415\text{ keV}} 6^+$ have been produced and the lifetime of the 6^+ level was determined. All the combinations of the relevant rings (N_n, N_m) with $n, m = 0, 1, 5, 6$ of GASP were used. For this lifetime the gate on the shifted component of the direct feeder is set to a smaller window due to the presence of the $12^- \xrightarrow{423\text{ keV}} 10^-$ transition in the spectrum (see fig.5.3). This transition does not really contaminate the $8^+ \xrightarrow{415\text{ keV}} 6^+$ decay but especially at the angles where the Doppler shift effect is maximum (ring 0 and 6) the transitions are very close in energy. The 351 keV transition is a contamination in the gated spectra for the shifted component of the transition under investigation in ring 0. For this reason only the intensities in rings 1, 5 and 6 are taken in account.

- For the lifetime of the 8^+ state the indirect method was used due to the presence of transition $14^- \xrightarrow{477\text{ keV}} 12^-$ which overlaps with the $10^+ \xrightarrow{476\text{ keV}} 8^+$ which directly feeds the 8^+ state.

Gated spectra were produced by gating on the shifted component of the transition $14^+ \xrightarrow{587\text{ keV}} 12^+$ only at backward angles. The presence of the transition $18^- \xrightarrow{591\text{ keV}} 16^-$ limits the use to the backward rings. In the gated spectra the intensities of the 415 keV depopulating transition and of the 475 keV populating transition have been determined.

- The presence of a contaminant transition in the negative parity side band populated in this reaction does not allow to use gates on the direct feeding transition $12^+ \xrightarrow{534\text{ keV}} 10^+$ of the 10^+ state because the $16^- \xrightarrow{535\text{ keV}} 14^-$ transition overlaps with the direct feeder of the level under investigation. Using the same arguments as for choice the gates in the case of the 8^+ state, the same gated spectra as those for 8^+ state were used here. The intensities of the shifted and unshifted components of both depopulating and populating transitions were determined.
- The direct gate method was used to determine the lifetime of the 12^+ state. The gated spectra produced by gating on the shifted component of the $14^+ \xrightarrow{587\text{ keV}} 12^+$ transition are used to determinate the lifetimes of the 8^+ and 10^+ states. In this case the gate is set on the shifted component of the direct feeder. The presence of the 530 keV transition in the gated spectra restricts the analysis to the ring 6 only.

Table 5.1 summarizes all the results which have been determined for levels in the gsb from different gates and in correspondence of different angles (rings of GASP). The final values of the lifetime τ of the level of interest is derived as the average of the lifetimes of the level at the different ring combinations.

Some attention has been payed to those lifetimes equal or smaller than the finite slowing down time of the ^{176}Os ions in the stopper. During the slowing-down in the stopper, the recoil does come at rest in a finite time interval. During this time interval the recoils velocity straggling is increased and its magnitude is decreasing with the subsequent emission of γ -rays [41]. Both the in-flight emission and the slowing-down emission contribute to the observation of the Doppler shifted γ -ray energy. To derive correction factors for the short lifetimes, the approach introduced in [41, 42] has been applied. In table 5.2 the corrected lifetimes are reported together with the lifetimes reported in the work [9]. These values have been measured with a dedicate DSAM experiment. The lifetime of 8^+ state is out of the subpicosecond range

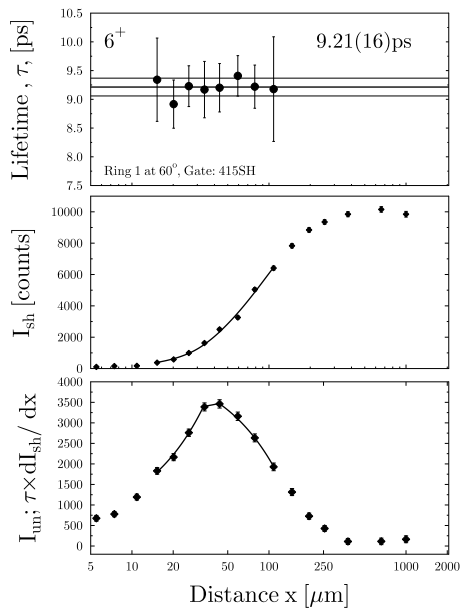


Figure 5.1: τ -plot and intensities of the shifted I_{sh} and unshifted I_{un} components of the transition $6_1^+ \rightarrow 4_1^+$ in ^{176}Os .

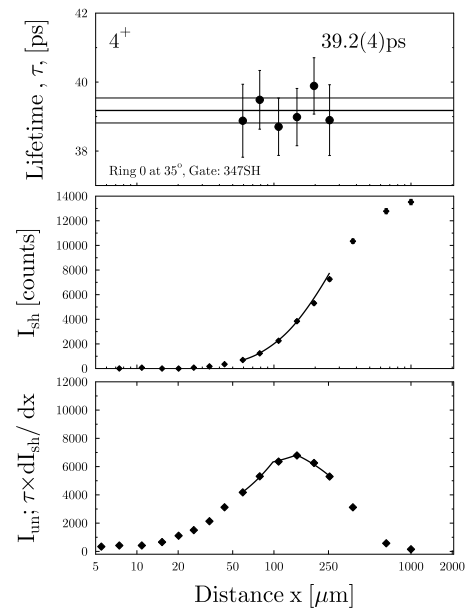


Figure 5.2: τ -plot and intensities of the shifted I_{sh} and unshifted I_{un} components of the transition $4_1^+ \rightarrow 2_1^+$ in ^{176}Os .

Table 5.1: Lifetimes of levels in the gsb of ^{176}Os at each ring-ring combinations. The first column indicates the gate used to determine these values. The label YYYSH indicates that the gate is set on the shifted component of the transition YYY.

Gate	τ_{ring}	4+ 260.3 keV	6+ 347.0 keV	8+ 415.0 keV	10+ 476.3 keV	12+ 533.8 keV
347SH	τ_0	40.44(33)ps				
	τ_1	39.18(36)ps				
	τ_5	48.9(5)ps				
	τ_6	42.13(42)ps				
415SH	τ_1		9.20(16)ps			
	τ_5		8.29(15)ps			
	τ_6		8.47(15)ps			
415UN	τ_6			3.40(10)ps		
	τ_5			3.51(11)ps		
587SH	τ_0			3.44(11)ps		
	τ_1			3.21(10)ps		
	τ_5			3.88(12)ps	1.23(15)ps	
	τ_6			3.26(10)ps	1.18(22)ps	0.56(15)ps

for the Doppler shift attenuation method and this lifetime is given with a big uncertainty. However, the agreement with the lifetimes of the state 8^+ 10^+ 12^+ extracted from this work is good as shown in the table 5.2. The mean time interval needed by the ^{176}Os recoils to come to rest in the stopper is calculated to be about 1.09(24)ps.

In table 5.6 the experimental final lifetimes values obtained in this work are compared with the lifetimes given in literature [3].

5.2 Lifetime of levels in the negative parity bands of ^{176}Os

Lifetimes of states in two side bands with negative parity have been determined.

To derive lifetimes of levels in both negative parity bands, the direct method has been used in most cases. A total of 6 lifetimes have been extracted. Details of the procedure used to derive these lifetimes are presented in the following. In figure 5.3 a partial level-scheme of ^{176}Os [40] is shown. The two bands under investigation are marked as neg-1 and neg-2.

Table 5.2: Lifetimes of levels in the gsb of ^{176}Os . The lifetime τ_{corr} corrected for the slowing down of the recoils in the stopper material is reported. In the last column the lifetimes known in literature τ_{lit} [9] are reported.

I^π	Energy [keV]	E_γ [keV]	τ [ps]	τ_{corr} [ps]	τ_{lit}
4 ⁺	395.5	260.3	40.4(6)	40.4(6)	
6 ⁺	742.3	347.0	8.56(30)	8.56(30)	
8 ⁺	1157.4	415.0	3.40(15)	3.40(15)	3.72(2.60)
10 ⁺	1633.8	476.3	1.20(20)	1.26 (21)	1.63(53)
12 ⁺	2167.8	533.8	0.56(22)	0.61(24)	0.70(21)

5.2.1 Analysis of the first excited band

Lifetimes of states with spin 9⁻ up to 13⁻ have been measured in the neg-1 band of ^{176}Os .

- For the lifetime of the 9⁻, the gates on the direct feeding transition $11^- \xrightarrow{398 \text{ keV}} 9^-$ could be employed without problems of contamination. The analysis of the depopulating transition was done using the gated spectra in all the relevant rings.
- The direct method was used to extract the lifetime of the 11⁻ level. Gated spectra were produced by gating on the shifted component of the $13^- \xrightarrow{464 \text{ keV}} 11^-$ which directly feeds the level under investigation. All the relevant rings have been used for gating but special care has been taken for ring 0 where the presence of the 471 keV transition of the ^{181}Ta is very close to the shifted component of the 464 keV. In this case a smaller gate window was chosen. Since no contamination was present in the gated spectra all the four relevant rings were employed for the analysis.
- To derive the lifetime of the 13⁻ level gates were set on the directly feeding transition $15^- \xrightarrow{519 \text{ keV}} 13^-$. Only the rings under forward angles were used because under backward angles the shifted component overlaps with the 511 keV line. No contamination was present. Therefore, for the analysis of the depopulating γ line, spectra from all four rings were employed.

The results of the analysis of the first excited band are summarized in table 5.4. In table 5.3 the lifetimes measured for levels in the gsb at each ring–ring combinations and for different gates are summarized.

Table 5.3: Lifetimes of levels in the two negative parity bands of ^{176}Os at each ring–ring combinations. The first column indicates also the gate used to determine these values. The label YYYSH indicates that the gate is set on the shifted component of the transition YYY.

Gate	τ_{ring}	9_1^+ 322.4 keV	11_1^+ 398.3 keV	13_1^+ 463.8 keV
398SH	τ_0	7.69(36)ps		
	τ_1	7.03(36)ps		
	τ_5	7.54(31)ps		
464SH	τ_0		3.46(16)ps	
	τ_1		3.35(17)ps	
	τ_5		3.55(18)ps	
	τ_6		3.39(19)ps	
519SH	τ_0			2.19(19)ps
	τ_1			2.2(2)ps
	τ_5			2.1(2)ps
	τ_6			1.9(2)ps
Gate	τ_{ring}	8_2^+ 313.2 keV	10_2^+ 374.4 keV	12_2^+ 422.9 keV
374SH	τ_0	6.7(7)ps		
423SH	τ_0		5.0(7)ps	
477SH	τ_0			4.7(3)ps

5.2.2 Analysis of the second excited band

The same criteria mentioned for the analysis of the neg-1 band have been adopted for the neg-2 band. Three lifetimes have been extracted corresponding to levels with spins from 8^- to 12^- . The obtained value are reported in table 5.4.

Table 5.4: Lifetimes of levels in the first and second excited band of ^{176}Os . The other data are taken from Nuclear Data. Sheets

I^π	Energy [keV]	E_γ [keV]	I_γ	σ_γ	τ [ps]
9_1^-	2075.7	322.4	100 (3)	E2	7.7 (4)
		442.2	31 (5)		
		918.4	30 (3)		
11_1^-	2473.7	398.3	6.4(13)		3.5 (2)
		306			
		839.7			
13_1^-	2937.1	463.8	<14		2.2 (2)
		768.9			
8_2^-	2020.8	313.2	100(3)	E2	6.7 (7)
		863.1	33		
10_2^-	2394.8	374.4	100	E2	5.0 (7)
12_2^-	2817.7	422.9	100	E2	4.7 (3)

5.3 The experiment at the Tandem in Cologne: lifetime of the first excited 2^+ in $^{178,176}\text{Os}$

As already mentioned two especially dedicated RDDS experiments were performed to measure the lifetime of the first excited state in the gsb of $^{178,176}\text{Os}$.

In literature the lifetimes of the first excited 2^+ states in $^{178,176}\text{Os}$ are known. O. Möller already measured the lifetimes with the delayed coincidence technique [3]. The lifetimes measured with this technique are 0.99(7)ns for the 2^+ in ^{178}Os and 1.21(18)ns for the 2^+ state in ^{176}Os .

The lifetime of the 2^+ state in ^{176}Os was measured only with a relative large experimental uncertainty and one might suspect that the measured lifetime is affected in addition by systematic error because the measured value of $\sim 1\text{ns}$ is at the limit of the technique employed in [3].

This suggest to remeasure the lifetime of the first excited 2^+ state in $^{178,176}\text{Os}$.

In table 5.5 the measured lifetimes from the RDDS experiments and the values given in literature are compared. Also included are the values of the delayed coincidence measurement using the double Orange spectrometer at the Cologne Tandem [50].

5.3.1 Lifetime of the 2^+ state in ^{178}Os

Spectra for the analysis of the first excited 2^+ level were created by gating on the shifted component of the direct feeding transition $4^+ \xrightarrow{266 \text{ keV}} 2^+$ in the rings 2 and 3.

Details about the experiment can be found in chapter 3. The resulting lifetime is 1.02(7)ns which is consistent with the lifetime measured with the delayed coincidence technique [3]. Some comments are required concerning the extraction of the lifetime of the level under investigation. In spite of the relatively small recoil velocity which causes a poor separation of the two components, the evolution of the in-flight and the stopped components while increasing the target-to-stopper distance are clearly visible, see fig 3.5. Only the detector at 0° were analyzed where the Doppler effect is more pronounced than in other rings.

5.3.2 Lifetime of the 2^+ state in ^{176}Os

To derive the lifetime of the 2^+ in the gsb of ^{176}Os , gates were set on the directly feeding $4^+ \xrightarrow{260 \text{ keV}} 2^+$ transition in the rings 3 and 2. In this measurement the recoil velocity was quite small too. Therefore the analysis has been focused on the ring at 0° where the Doppler effect is more pronounced than in the other rings.

Table 5.5: Lifetimes of the first excited 2^+ of $^{176,178}\text{Os}$. The experimental results are compared with the lifetime τ_{lit} measured by O. Möller [3] and the lifetimes τ_{ee} measured with the Double Orange [50].

Nucleus	I^π	E_γ [keV]	τ [ns]	τ_{lit} [ns]	τ_{ee} [ns]
^{178}Os	2^+	132.4	1.02 (3)	0.99 (7)	1.05 (5)
^{176}Os	2^+	135.1	0.92 (13)	1.21 (18)	0.88 (3)

As cross check of the lifetimes obtained with the RDDS method, two dedicated experiments were performed [50] using the Double Orange Spectrometer at the FAN Tandem of the University of Cologne. In table 5.5 the lifetime of the first excited 2^+ in $^{176,178}\text{Os}$ measured in this work with the RDDS method, the e^-e^- coincidence method τ_{ee} and the values given in literature τ_{lit} [3] are summarized.

Table 5.6: Measured lifetimes and transition probabilities in the ground state band of ^{176}Os . The other data are taken from Nuclear Data Sheets.

I^π	Energy [keV]	E_γ [keV]	I_γ	σ_γ	τ [ps]	B(E2) [$e^2\text{fm}^4$]	B(E2) [W.u.]
2^+	135.1	135.1	100	E2	915(30)	8451(287)	144(5)
4^+	395.5	260.3	100	E2	40.4(6)	14140(160)	243 (5)
6^+	742.3	347.0	100	E2	8.56(30)	17870 (150)	305 (11)
8^+	1157.4	415.0	100	E2	3.40(15)	18800^{+870}_{-800}	321^{+15}_{-14}
10^+	1633.8	476.1	100	E2	1.26(21)	25810^{+5160}_{-3690}	441^{+88}_{-63}
12^+	2167.8	533.8	100	E2	0.61(24)	30310^{+1970}_{-850}	517^{+336}_{-146}

In table 5.6 the determined lifetimes of levels in the gsb of ^{176}Os are given together with the transition probabilities calculated from the experimental lifetimes measured in this work.

5.4 Lifetimes in ^{177}Os

A CASCADE calculation revealed that other reaction channels with smaller cross sections were open in the GASP experiment. As example the $4n$ channel which corresponds to the population of states in ^{177}Os with a cross section of about 8% of the total fusion cross section at a beam energy of 150MeV as predicted by the CASCADE calculation.

It was possible for this reaction channel to extract lifetime of the $\frac{9}{2}^-$, $\frac{13}{2}^-$ and $\frac{17}{2}^-$ states in ^{177}Os . The results are given in Table 5.7 and compared with the lifetimes measured by O. Möller [51]. The same criteria mentioned for the analysis of ^{176}Os have been adopted for the lifetimes in ^{177}Os .

Table 5.7: Measured lifetimes of the first excited $\frac{9}{2}^-$, $\frac{13}{2}^-$ and $\frac{15}{2}^-$ states in ^{177}Os . The experimental results are compared with the lifetime τ^\dagger measured by O. Möller [51]. The other data are taken from the Nuclear Data Sheets

I^π	Energy [keV]	E_γ	I_γ	σ_γ	τ [ps]	τ^\dagger [ps]
$\frac{9}{2}^-$	285.1	194.5	100	E2	110(9)	110(5)
$\frac{13}{2}^-$	567.5	282.4	100	E2	26.6(1.8)	23.3(9)
$\frac{17}{2}^-$	924.9	357.4	100	E2	6.6(5)	6.67(20)

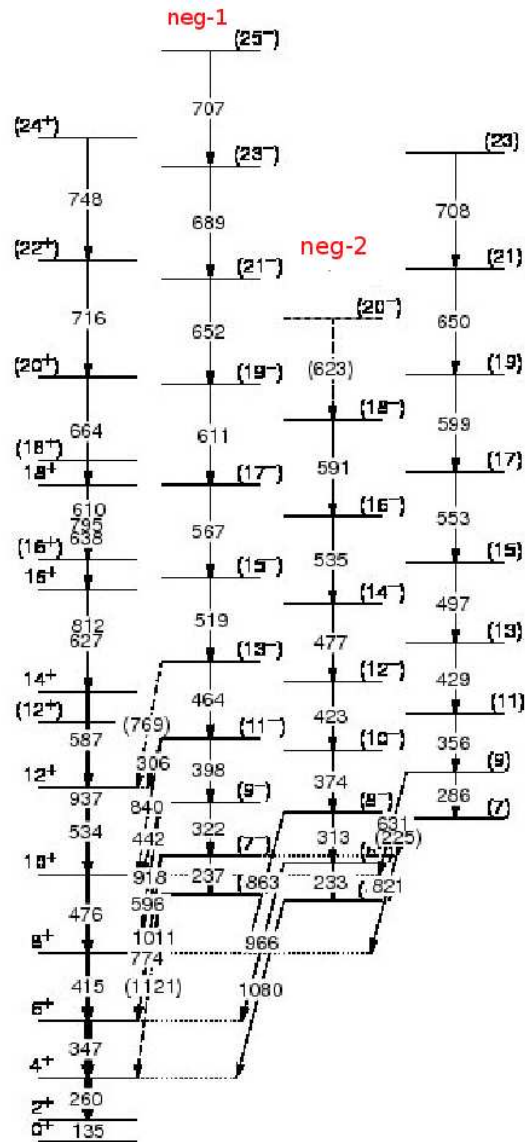


Figure 5.3: Partial level scheme of ^{176}Os [40]. The two side bands with negative parity which are investigated in this work are marked as neg-1 and neg-2.

Chapter 6

Comparison with the models and discussion

The use of collective observables to describe the behavior of complex systems like the nucleus is a helpful method to provide information for the study of the nuclear many-body problem. Information on the shape of the nucleus can be extracted from these observables.

Some of the empirical observables which will be used in this work to discuss a change in the structure are briefly introduced here.

The ratio $R_{4/2} = \frac{E(4_1^+ \rightarrow 0_1^+)}{E(2_1^+ \rightarrow 0_1^+)}$ gives directly the basic structure of the nucleus: near closed shell $R_{4/2} < 2$, vibrational for $R_{4/2} \sim 2.0$, transitional for $R_{4/2} \sim 3.0$ and rotational for $R_{4/2} \sim 3.33$. The ratio $R_{4/2}$ value is thus interesting if one wants to discuss changes in shape. It can be used as starting point for determining the structure of a particular nucleus but information on other low-lying states must also be considered.

Other observables which act as sensitive signatures of the structure are the transition strengths. The energy of the 2_1^+ state for example and the $B(E2 : 2_1^+ \rightarrow 0_1^+)$ give the overall scale of collectivity and, for deformed nuclei, the value of the deformation β . As the collectivity increases (i.e. the number of valence nucleons increases) also the $B(E2 : 2_1^+ \rightarrow 0_1^+)$ grows¹. The E2 strength of the $4_1^+ \rightarrow 2_1^+$ transition also increases in the spherical-to-deformed transition but the ratio of energies $R_{4/2} = \frac{E(4_1^+)}{E(2_1^+)}$ decreases.

Transition strengths between different bands are sensitive to shape changes too.

Several models have been developed with the aim to describe the nucleus using a geometrical description of the shape. Free parameters contained

¹B(E2) values are very small near doubly magic numbers, it reach a peak near mid-shell and decreases again near the next doubly magic region.

in these models are adjusted to specific nuclei and the shape evolution is described by varying the properties of the ground state and of low-lying levels with the parameters of the models [20].

The transition probabilities values derived in the present work allow one to extract nuclear structure information characterizing the collective motion of the gsb and the first excited band in ^{176}Os . The comparison of the experimental results presented in the fifth chapter and the outcome of the theoretical models predictions described in the first chapter is discussed in this chapter.

6.1 The nucleus ^{176}Os

Recently, as already mentioned in this thesis, the first nucleus outside from the well established $A \sim 150$ ones region showing X(5) features has been found [8, 51]. The nucleus ^{178}Os is indeed the first example of an X(5) - like nucleus in the mass region $A \sim 180$. Of course, this first result motivates investigations in neighboring nuclei. The attention was focused on the even – even neighbors ^{176}Os and ^{180}Os . In this work only the lighter osmium isotope has been investigated.

The nucleus ^{176}Os , with $Z = 76$ and $N = 100$ is 6 valence protons away from the closure of the shell at $Z = 82$ and is located at about half way between closed shells at $N = 82$ and $N = 126$. From this point of view ^{176}Os can be considered a promising candidate. In order to find other regions where X(5)-like nuclei can be found, it appears reasonable to look where fast transitions from spherical to axially symmetric deformation are expected. Thus regions around mid-shell for nucleons of one type with few valence of nucleons of the other type are the most promising ones for finding X(5) type nuclei [8]. The nucleus ^{176}Os is located in a region which presents the above mentioned characteristics.

In figure 6.1 a portion of the energy spectrum of ^{176}Os which includes the ground state band and the β band is shown as well as the X(5) predicted spectrum for the $s = 1, 2$ bands according to the X(5) terminology. The normalized energy of levels in the gsb of ^{176}Os are presented in figure 6.2 compared with those of the X(5)-like nuclei ^{178}Os and ^{152}Sm , ^{150}Nd and with the predictions of the models. Table 6.3 reports the energy ratios of levels in $^{176,178}\text{Os}$ isotopes which are compared to the values found for some of the well known X(5)-like nuclei and to the predictions of the X(5) model. In table 6.2 the relative transition strengths in ^{176}Os are compared to the X(5) predictions and to the values in ^{178}Os .

Of special importance are also the transition probabilities within the first

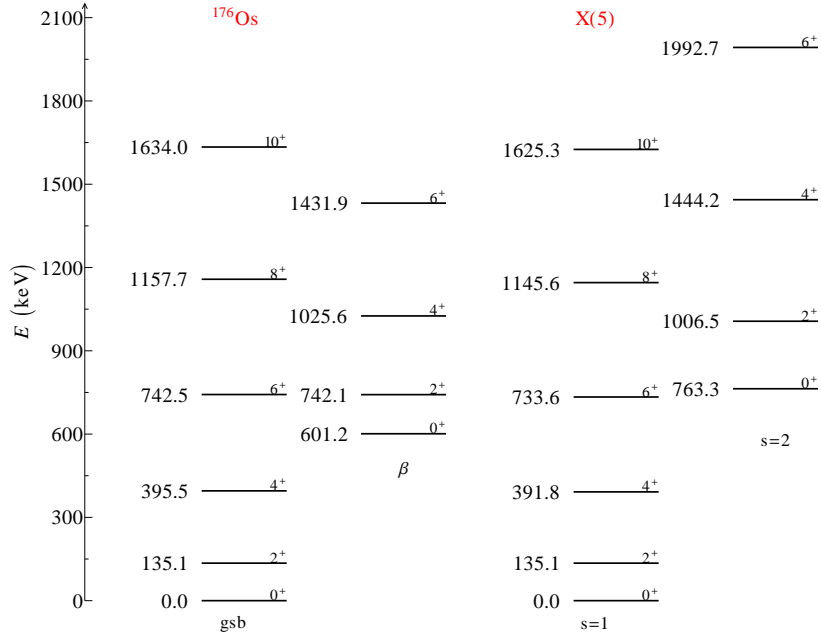


Figure 6.1: Partial level scheme of ^{176}Os (gsb and β band) compared with the predictions of the $s = 1, 2$ bands of the X(5) model. Energies are in (keV) and normalized to the experimental $E(2^+)$ value.

excited band ($s = 2$ in the X(5) terminology) and those of interband transi-

I^π	X(5)	^{178}Os	^{176}Os
$E(4_1^+)/E(2_1^+)$	2.91	3.01	2.92
$E(6_1^+)/E(2_1^+)$	5.43	5.75	5.49
$E(8_1^+)/E(2_1^+)$	8.48	9.01	8.57
$E(10_1^+)/E(2_1^+)$	12.03	12.7	12.09

Table 6.1: Energy ratios of levels in the gsb of ^{178}Os and ^{176}Os with the corresponding X(5) values. All the values are relative to the energy of the 2^+ . The energy values are taken from NDS [52].

I^π	X(5)	^{178}Os	^{176}Os
2^+	1.00	1.00	1.00
4^+	1.58	1.64	1.71
6^+	1.98	2.10	2.15
8^+	2.27	2.37	2.26
10^+	2.61	2.78	3.10

Table 6.2: $B(E2; I \rightarrow I - 2)$ normalized to the $B(E2; 2_1^+ \rightarrow 0_1^+)$.

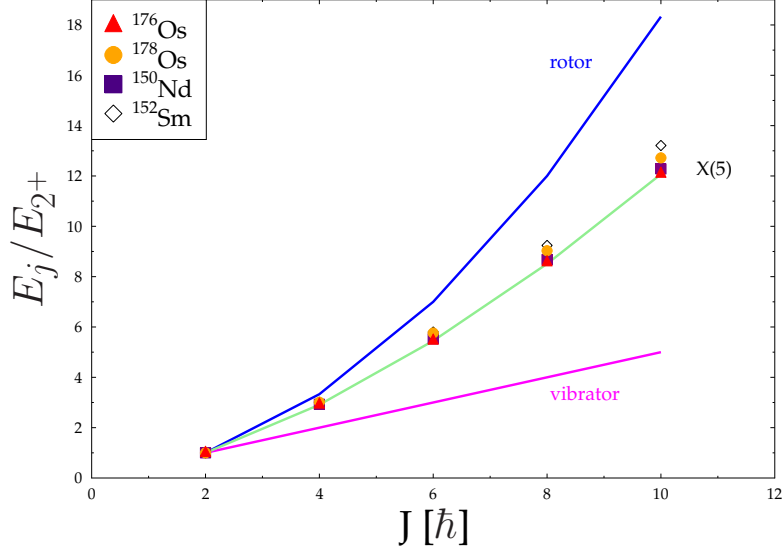


Figure 6.2: Normalized energy levels of the yrast band for the $^{176,178}\text{Os}$, ^{150}Nd and ^{152}Sm . The values are compared with the predictions of the theoretical models. The experimental energies are taken from NDS

tions between the $s=2$ and the gsb ($s=1$). In the framework of the X(5) model, the interband transition strengths $I_{s=2} \rightarrow (I+2)_{s=1}$ are expected to be larger than $I_{s=2} \rightarrow I_{s=1}$ ones, and the $I_{s=2} \rightarrow (I-2)_{s=1}$ transition strengths are one order of magnitude smaller than the latter ones. In table 6.2 the relative transition strengths within the ground-state band of ^{176}Os are compared to the X(5) predictions and to the values of ^{178}Os .

Information concerning the band S2 in ^{176}Os can be found in the work [53]. The excited band was populated by the beta decay of ^{176}Ir . In table 6.4 the experimental transition strengths of $^{176,178}\text{Os}$ [53] and the values predicted by the X(5) model are given for comparison. All the intensities are normalized to the intensity of the transition $I_2^+ \rightarrow (I-2)_2^+$.

The energy position of the band-head of the $s=2$ and $s=3$ band of the spectrum predicted by the X(5) model can be compared with the position of β and γ band-head of the experimental spectrum to check if the nucleus presents the features of the X(5) symmetry. In the X(5) predictions the $s=2$ (β) band-head is located at lower energy than that of the $s=3$ (γ) band-

Table 6.3: Comparison of the energy ratios of levels in Os isotopes to the prediction of the X(5) model and to the known X(5)–like nuclei ^{154}Gd [4] and ^{152}Sm [20].

Energy ratio	^{176}Os	^{178}Os	^{180}Os	^{154}Gd	^{152}Sm	X(5)
$E(4_1^+)/E(2_1^+)$	2.93	3.01	3.09	3.01	3.01	2.91
$R(4/2)_{S_2}^\dagger$	3.00	3.09	3.43	2.71	2.69	2.80
$E(0_2^+)/E(2_1^+)$	4.45	4.91	5.57	5.53	5.62	5.67
$R(2_{S_2}/2_{S_1})^\ddagger$	1.05	0.91	1.02	1.10	1.03	1.80

\ddagger with $R(2_{S_2}/2_{S_1}) = (E(2_2^+) - E(0_2^+))/E(2_1^+)$

\dagger with $R(4/2)_{S_2} = (E(4_2^+) - E(0_2^+))/(E(2_2^+) - E(0_2^+))$

head. In both spectra of the $^{176,178}\text{Os}$ nuclei, the band-head of the β – band lies at lower energy than that of the γ band.

The energy ratios of levels in Os – isotopes summarized in table 6.3, are compared to the prediction of the X(5) model and to the known X(5)–like nuclei ^{154}Gd [4] and ^{152}Sm [20]. All except for the $E(2_2^+)/E(2_1^+)$ value is reproduced.

It can be deduced from the comparison of the energy spectra and the relative transition strengths with the predictions of the X(5) model, that the even – even nucleus ^{176}Os is a promising X(5) candidate.

6.1.1 ^{176}Os as X(5) nucleus

In this work the absolute B(E2)–values in the ground state band were determined from the experimental lifetimes. These values allow for a stringent test of the X(5) predictions together with the comparison of the energy spectra. The experimental observables are compared with the Iachello’s approximate X(5) solution and the exact X(5) numerical solution of Caprio (see paragraph 1.3.2).

Comparison to the X(5) approximate solution

In figure 6.3 the transition quadrupole moments within the gsb of ^{176}Os are plotted versus the spin and compared with the theoretical values of the X(5) model [2] approximation, the symmetric rotor [SU(3)] and the IBA U(5) limit. The transition quadrupole moments Q_t are calculated with relation

Table 6.4: Comparison of the relative transition probabilities of the X(5) predictions from [2] with the experimental values in $^{176,178}\text{Os}$. The intensities are normalized to the intensity of the transition $I_2^+ \rightarrow (I-2)_2^+$. The γ^- intensities are taken from [53].

	^{178}Os	^{176}Os	X(5)
$2_2^+ \rightarrow 0_1^+$	0.02(1)	n.o.	3
$\rightarrow 2_1^+$	0.4(1)	4.8(5)	10
$\rightarrow 4_1^+$	0.9(1)	53(8)	46
$\rightarrow 0_2^+$	100	100	100
$4_2^+ \rightarrow 2_1^+$	0.2(1)	0.01(1)	0.8
$\rightarrow 4_1^+$	11(1)	9.7(5)	5
$\rightarrow 6_1^+$	50(16)	52(18)	23
$\rightarrow 2_2^+$	100	100	100
$6_2^+ \rightarrow 4_1^+$	0.10(3)	0.8(1)	0.4
$\rightarrow 6_1^+$	19(2)	15(1)	3.3
$\rightarrow 8_1^+$	n.o.	n.o.	15
$\rightarrow 4_2^+$	100	100	100

1.8 from the experimental $B(E2)$ transition strengths. The experimental Q_t value for the $2_1^+ \rightarrow 0_1^+$ transition is used as normalization factor for the theoretical predictions. The agreement of the experimental data with the X(5) predictions is found to be good and comparable to that found for the X(5) examples ^{150}Nd [6] and ^{154}Gd [4].

To illustrate the quality of the results obtained in this work, in Fig. 6.4 the Q_t -plot of two well known X(5)-like nuclei in the $N = 90$ isotones and the first example of the X(5)-like nucleus outside the $A = 150$ mass region are compared to the result obtained in this work for ^{176}Os .

As mentioned, from the transition strength $B(E2; 2_1^+ \rightarrow 0_1^+) = 0.83e^2b^2$ a value of $Q_0 = 6.5eb$ is derived. From the comparison of the partial level schemes in figure 6.1 it is evident that the X(5) symmetry predicts correctly the relative energies in the gsb sequence, while there is a disagreement between the energies in the sequence on the 0_2^+ . Indeed the experimental levels are much closer in energy to each other compared to the X(5) model. The reason can be related back to the fact the potential in β is assumed to be an

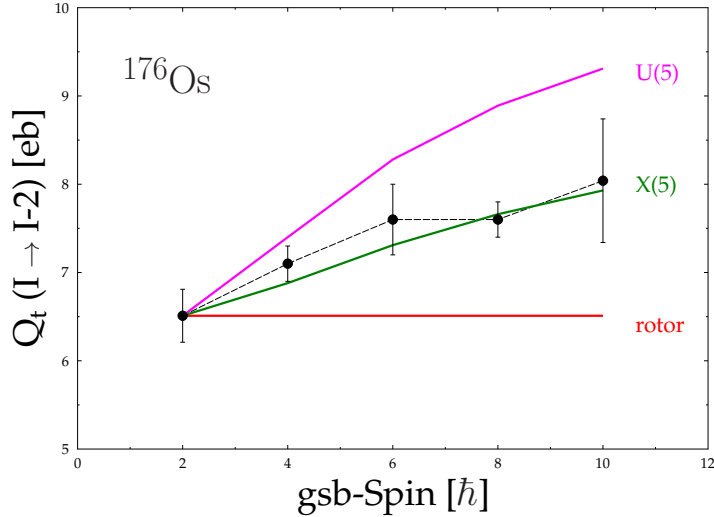


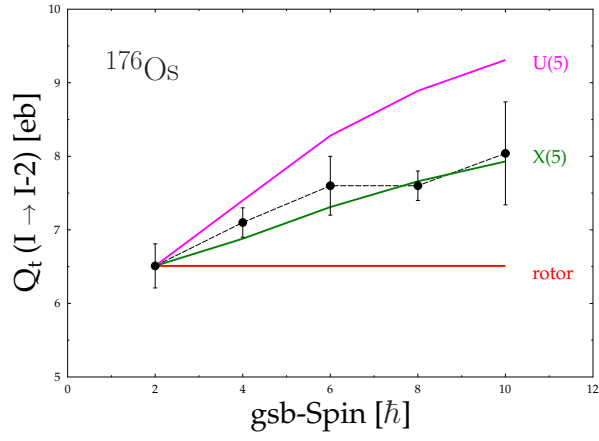
Figure 6.3: Transition quadrupole moments in the ground state band of ^{176}Os . The measured values are compared to the expected ones for the rigid rotor, the X(5)-like nucleus in the approximate case and the U(5) limit of the IBA.

infinite square well. By changing the potential with a sloped well, the effect of this potential will be minimal on the low-lying (yrast) states while the high energy states will have lower energies [54]. It is important to mention again that the X(5) model does not have free parameters and has only two scaling parameters for energies and the $B(E2)$ values.

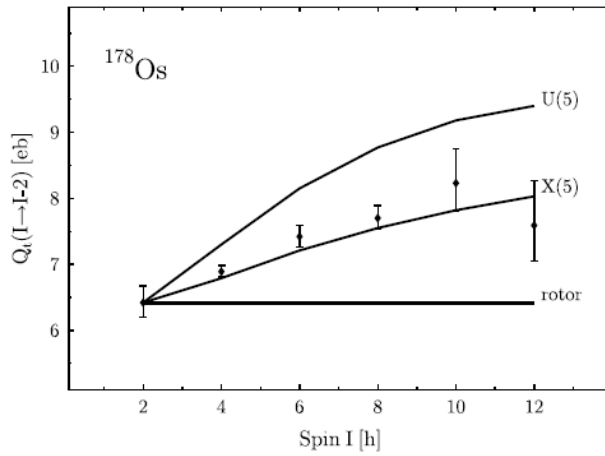
Comparison to the X(5) exact numerical solution

In figure 6.5 the comparison of the partial experimental level scheme of ^{176}Os with the exact spectra for the X(5) potential with the γ -stiffness parameter $a = 200$ ² proposed by Caprio M.A. [27] is presented. In the exact numerical X(5) solution energies and transition rates are given for the $s=1$, $s=2$ and $s=3$ bands using the X(5) terminology. The gsb, β and γ - band of the experimental spectrum can be compared with $s=1$, $s=2$ and $s=3$ bands, respectively. In the experimental and theoretical spectra, the ener-

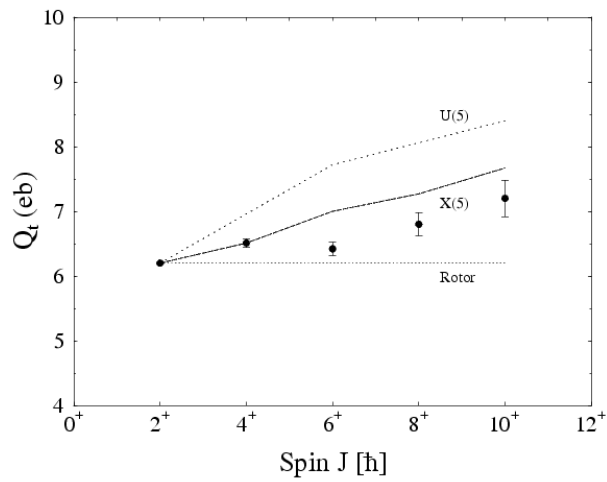
²In the vicinity of the γ stiffness $a = 200$, the approximate results quantitatively resemble the exact results.



(a)



(b)



(c)

Figure 6.4: Comparison of the Q_t -values in the gsb of ^{176}Os (a) with well known X(5)-like nuclei ^{154}Gd (c)[4] and the X(5)-like nucleus ^{178}Os [8, 51].

gies of the levels and the energies of the intraband transitions normalized to $E(2_1^+ \rightarrow 0_1^+) = 100$ are given. The experimental and predicted B(E2) transition strengths in the gsb, normalized to the $B(E2; 2_1^+ \rightarrow 0_1^+) = 100$, are given for direct comparison. B(E2) transition rates for the intra and inter-band transitions in the β and γ bands are summarized in table 6.5.

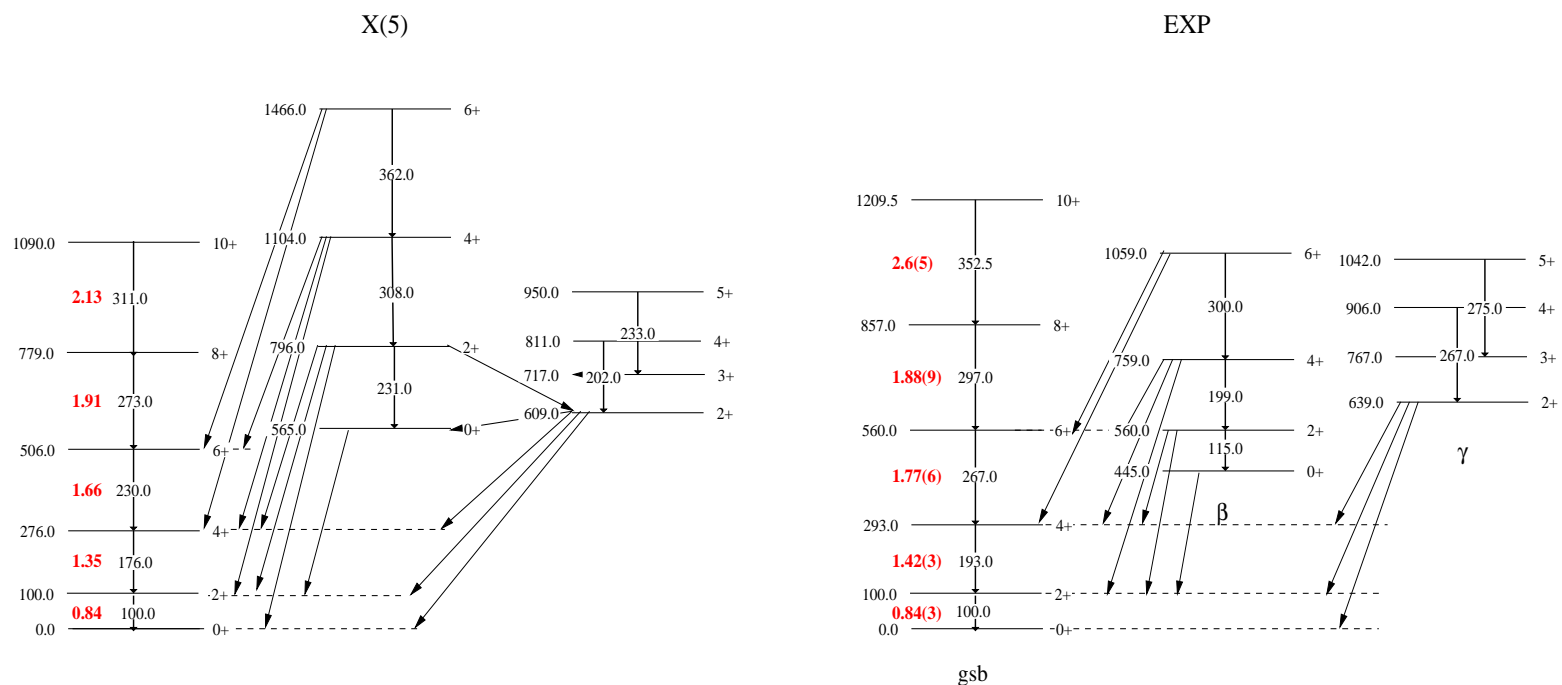


Figure 6.5: Experimental level scheme and B(E2) transition strengths (in e^2b^2) compared to the X(5) exact numerical solution. Energies presented are in keV.

Table 6.5: Comparison of the relative transition intensities of the exact numerical $X(5)^\dagger$ and approximate $X(5)$ predictions [2, 27] with the experimental values in ^{176}Os . The γ -intensities for the interband transitions are taken from [53].

	$X(5)^\dagger$	^{176}Os	$X(5)$
$2_2^+ \rightarrow 0_1^+$	3	n.o.	3
$\rightarrow 2_1^+$	4.9	4.8(5)	10
$\rightarrow 4_1^+$	37	53(8)	46
$\rightarrow 0_2^+$	100	100	100
$4_2^+ \rightarrow 2_1^+$	1.1	0.01(1)	0.8
$\rightarrow 4_1^+$	1.7	9.7(5)	5
$\rightarrow 6_1^+$	18	52(18)	23
$\rightarrow 2_2^+$	100	100	100
$6_2^+ \rightarrow 4_1^+$	0.7	0.8(1)	0.4
$\rightarrow 6_1^+$	1.0	15(1)	3.3
$\rightarrow 8_1^+$	-	n.o.	15
$\rightarrow 4_2^+$	100	100	100
$2_3^+ \rightarrow 0_2^+$	0.83	n.o.	7.6
$\rightarrow 2_1^+$	100	100	100
$\rightarrow 4_1^+$	2.1	85(20)	5
$\rightarrow 0_1^+$	23.3	27(5)	64

From the comparison of the partial level schemes it can be deduced that the energies and $B(E2)$ transition strengths within the gsb are quite good reproduced by the model. The disagreement in the energy spacing of levels in the β band, observed in the approximate $X(5)$ solution, still remains. It is to be noted is that the band head of the β band in the experimental spectrum is located at a lower energy with respect to the value predicted by the model.

The exact solution of Caprio supplies also information on the γ band ($s=3$) as well as the intraband and interband transition rates with the gsb ($s=1$) and β ($s=2$) band. This allowed a more stringent test to find the characteristic features of the $X(5)$ symmetry. The agreement between the energies in the γ band predicted by the model and the experimentally observed energies is quite good showing a discrepancy smaller than 10%. Also the interband $B(E2)$ transition strengths, summarized in table 6.5 are quite

well reproduced by the model.

6.2 The comparison with the theoretical models IBA and GCM

One must remark that perfect agreement of the experimental data with the X(5) predictions is of course not observed. The X(5) model does not allow any fitting and uses only two scaling parameters for the energies and the B(E2) values. Therefore one should expect an improved agreement between experimental and theoretical values when using other theoretical models where the calculated quantities can be adjusted by varying model parameters. With the aim of reproducing the spectroscopic properties of the nucleus ^{176}Os , two calculations have been performed: a GCM fit and a IBM-1 fit with a valence boson number $N = 12$. The results are shown in figures 6.6 and 6.7. The transition strengths (in e^2b^2) for the gsb obtained from the fits are given in the figure for an immediate comparison, while the interband transition strengths are summarized in table 6.6 and compared with the experimental values.

The experimental data of ^{176}Os has been fitted in the framework of the IBM-1 model [16]. This fit helps also to position the nucleus in the transitional region between spherical nuclei and deformed nuclei. The results of the fit are presented in figure 6.6 and the parameters of the fit summarized in table 6.7. Only two terms of the Hamiltonian 1.11, namely the boson number operator and the quadrupole operator, were used.

The overall agreement with the experimental data of ^{176}Os is relatively good. The calculations provide a reasonable description of the low-lying spectra. The spacing in the gsb are described almost exactly while the energies of the γ -band are reproduced to within 6-15%. The energy spacing of levels in the sequence on the 0_2^+ state is lower in the experimental data than in the calculations but the location of the 0_2^+ is well described. It is not surprising that this spacing is not reproduced since it is difficult to reproduce by other collective models too. The IBM-1 model with two parameters fails in the reproduction of the transition probabilities, indeed the predicted B(E2) transition rates between the high spin states of gsb are underestimated within 20-40%.

Table 6.6: The relative transition probabilities of transition between the β , γ and gsb in ^{176}Os . The intensities are normalized to the intensity of the strongest transition. The experimental γ -intensities are taken from [53].

	GCM	^{176}Os	IBM
$2_2^+ \rightarrow 0_1^+$	-	n.o.	-
$\rightarrow 2_1^+$	15	4.8(5)	11.1
$\rightarrow 4_1^+$	26	53(8)	7
$\rightarrow 0_2^+$	100	100	100
$4_2^+ \rightarrow 2_1^+$	0.002	0.01(1)	0.1
$\rightarrow 4_1^+$	8.7	9.7(5)	5.6
$\rightarrow 6_1^+$	13	52(18)	0.7
$\rightarrow 2_2^+$	100	100	100
$6_2^+ \rightarrow 4_1^+$	0.001	0.8(1)	0.05
$\rightarrow 6_1^+$	7	15(1)	4
$\rightarrow 8_1^+$	-	n.o.	-
$\rightarrow 4_2^+$	100	100	100
$2_3^+ \rightarrow 2_1^+$	100	100	100
$\rightarrow 0_1^+$	98	27(5)	96
$\rightarrow 4_1^+$	24	85(20)	12
$\rightarrow 0_2^+$	-	n.o.	-

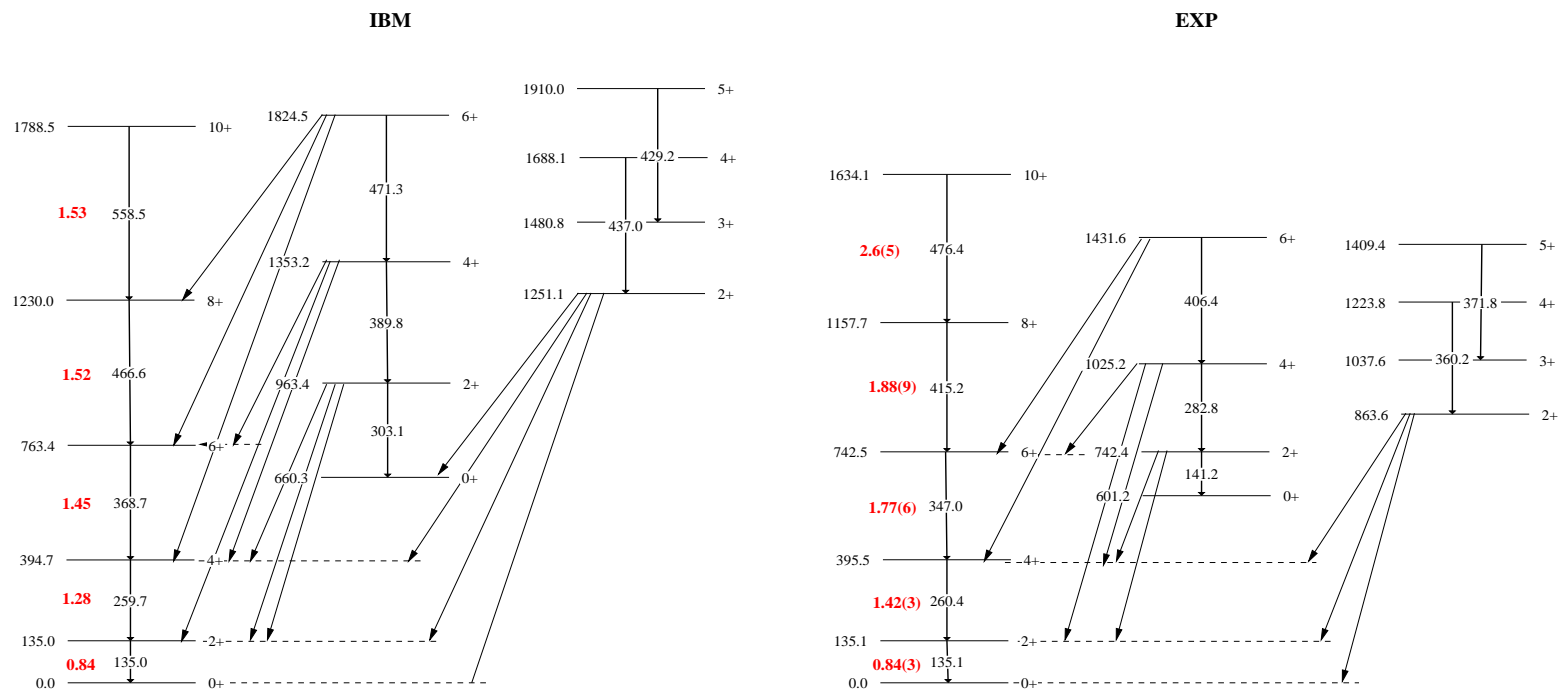


Figure 6.6: . Experimental level scheme and $B(E2)$ transition strengths (in e^2b^2) compared to the IBM-1 fit. Energies presented are in keV.

The GCM calculation is performed using the code developed by Trolteiner et al.[55] with the aim of reproducing the spectroscopic properties of ^{176}Os and deriving information on the collective potential $V(\beta, \gamma)$. The fit in the frame of the General Collective Model is performed with six parameters (see eq. 1.9). The results are presented in figure 6.7 and compared with the experimental data. The agreement is found to be very good for the gsb. The energy spacing in the β and γ bands are quite well reproduced, however, the two band heads are at higher energies with respect to the experimental data. The intraband B(E2) transitions are well reproduced by the model as well as the interband transitions for the β and γ which are reported in table 6.6. As expected a better agreement is obtained in the framework of GCM compared with the X(5) model framework.

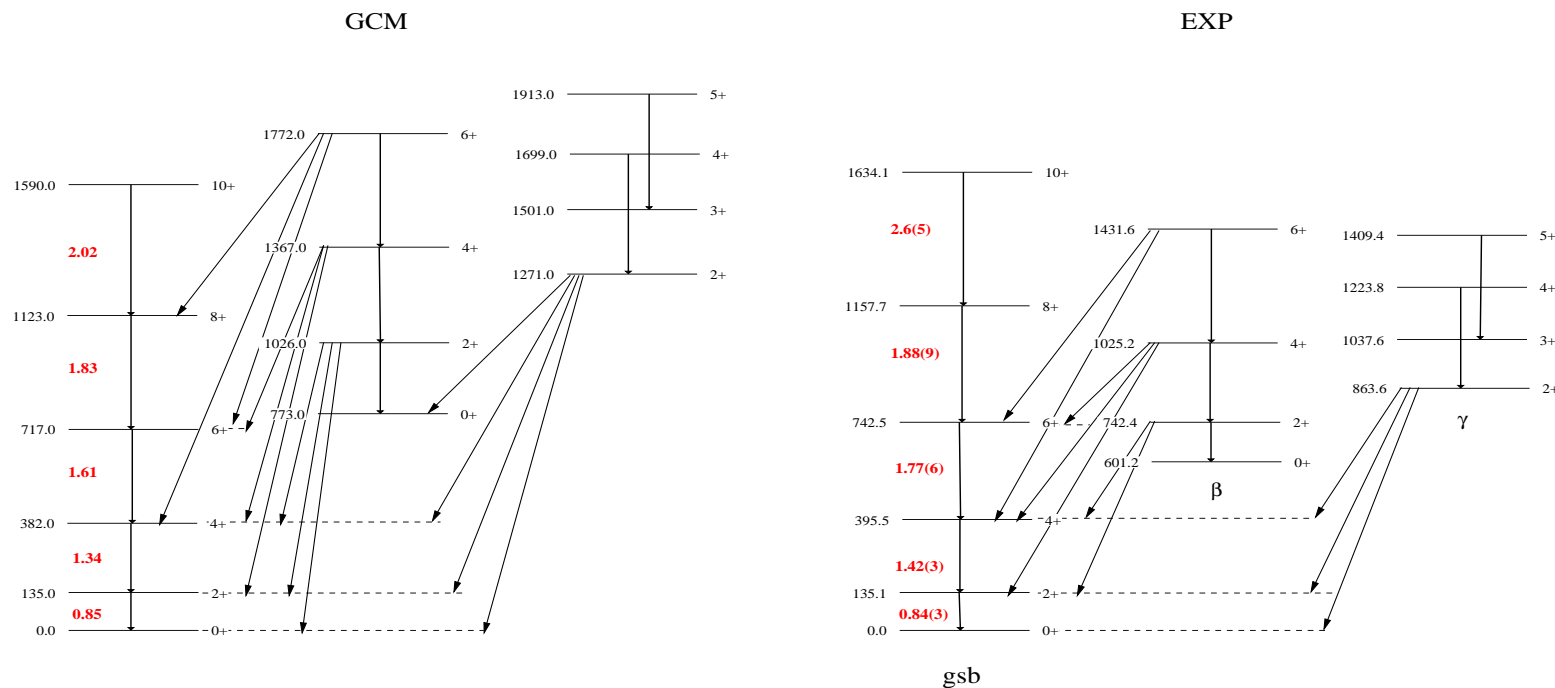


Figure 6.7: . Experimental level scheme and B(E2) transition strengths (in e^2b^2) compared to the GCM fit. Energies presented are in keV.

In figure 6.8 the results obtained in this work are summarized and graphically represented. The experimental energy ratios (a) and the normalized experimental transition probabilities (b) for the ground state sequence (up to spin $j = 10$) are plotted versus spin together with those predicted by the X(5) model, IBM and GCM. The rotor and vibrator limits are also given for comparison. The experimental energy spectrum of the nucleus ^{176}Os is satisfactorily reproduced by X(5), IBM and GCM model. The transition probabilities within the gsb are satisfactorily reproduced by both X(5) mode and GCM while the IBM-1 fails.

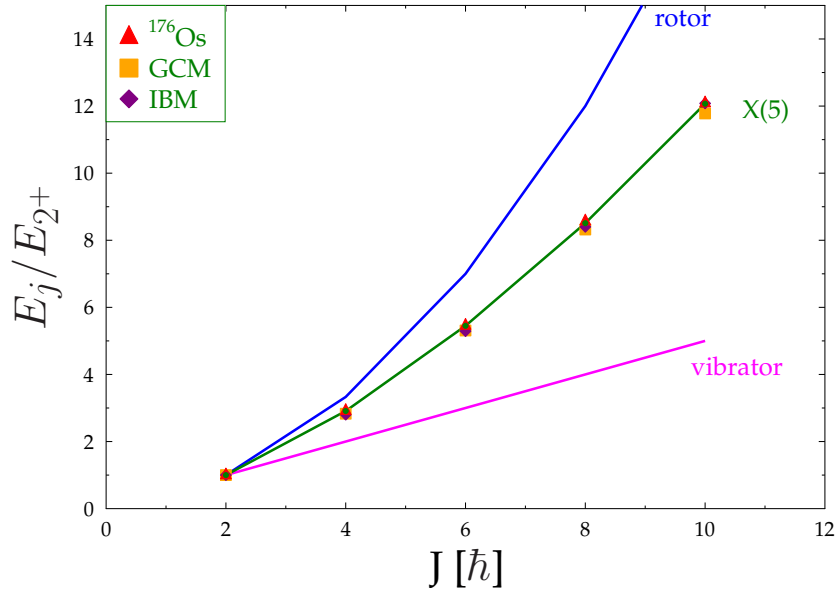
In figure 6.9, the experimental energy ratios (a) and the transition probabilities (b) of the X(5) like nuclei ^{178}Os and ^{176}Os , are plotted together with those of two well known X(5)-like nuclei, ^{150}Nd and ^{152}Sm . The results of the present work on the investigation on the nuclear structure of the low-lying states in the ^{176}Os nucleus is found to be good and comparable to that found for the X(5) examples ^{150}Nd [6] and ^{152}Sm [20].

The General Collective Model provides the possibility for investigating the role of the collective degrees of freedom β and γ . In figure 6.10 and 6.12 the GCM potentials derived from the fit of ^{176}Os are presented and compared with the potentials of the nucleus ^{154}Gd obtained from a GCM fit [4]. The potentials are similar but nevertheless some differences exist. The potential in β is more expanded in ^{154}Gd while the potential in ^{176}Os shows a larger depth. The two potentials in γ are very similar but a larger prolate-oblate energy difference is observed in ^{176}Os .

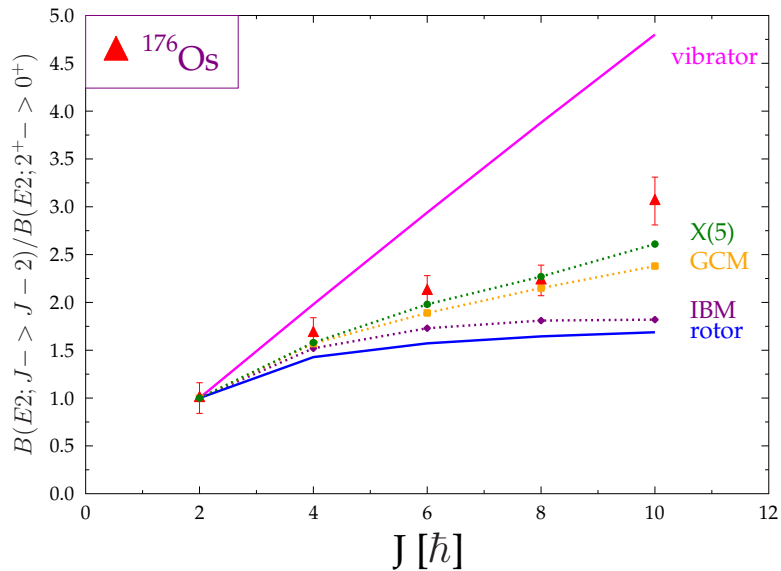
Table 6.7: Parameters of the IBM-1 and GCM fits for ^{176}Os .

IBM		GCM					
η	χ	B_2 [MeV s ²]	P_3 [MeV s ²]	C_2 [MeV]	C_3 [MeV]	C_4 [MeV]	D_6 [MeV]
0.76	$-1.0\frac{\sqrt{7}}{2}$	67.47×10^{-42}	7.48×10^{-44}	-174.8	310.1	3547.4	3710.4

The IBA fit discussed in this section enables a comparison with the X(5) symmetry. The parameter space for the Hamiltonian given by equation 1.16 is generally represented by a triangle [18], called Casten triangle, with one IBA dynamical symmetry at each vertex. The Casten triangle is represented in figure 6.2. The X(5) critical point is indicated as corresponding to the first-order phase transitional point on the U(5)-SU(3) axis at ($\eta = 0.75$, $\chi = -\sqrt{7}/2$). In the triangle also the position of the ^{176}Os in this parameter space ($\eta = 0.76$, $\chi = -1.0\sqrt{7}/2$), deduced from the IBA fit of the experimental

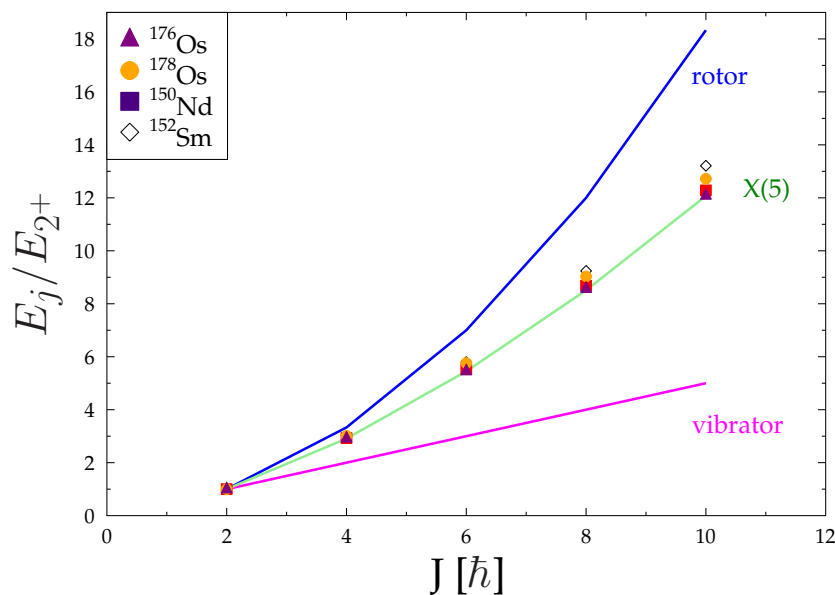


(a)

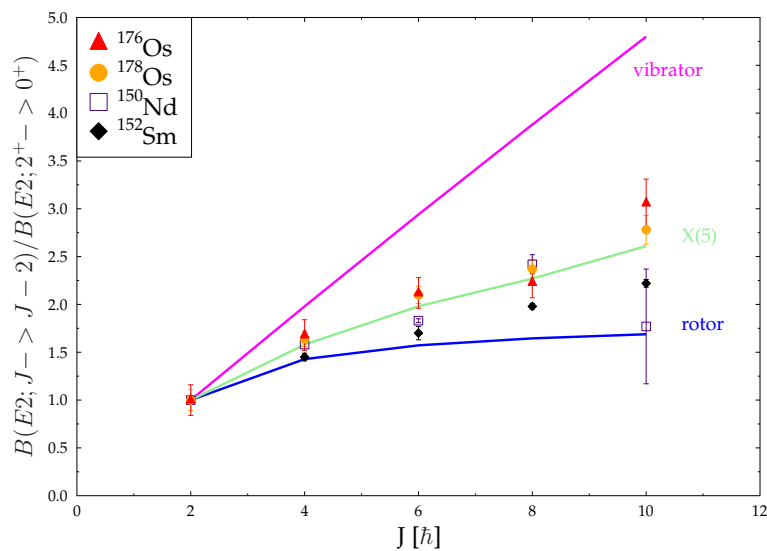


(b)

Figure 6.8: Experimental energy ratios (a) and the normalized experimental transition probabilities (b) for the ground state sequence (up to spin $j = 10$) in ^{176}Os are plotted versus spin together with those predicted by the X(5) model, IBM and GCM. The rotor and vibrator limits are also given for comparison.



(a)



(b)

Figure 6.9: experimental energy ratios (a) and the transition probabilities (b) of the X(5) like nuclei ^{178}Os and ^{176}Os , are plotted together with those of two well known X(5)-like nuclei, ^{150}Nd [6] and ^{152}Sm [20].

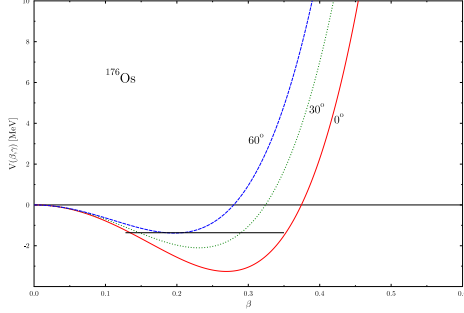


Figure 6.10: Projection of the GCM potential $V(\beta, \gamma)$ for ^{176}Os with $\gamma = 0^\circ, 30^\circ$ and 60° . The position of the ground state is indicated by the horizontal line.

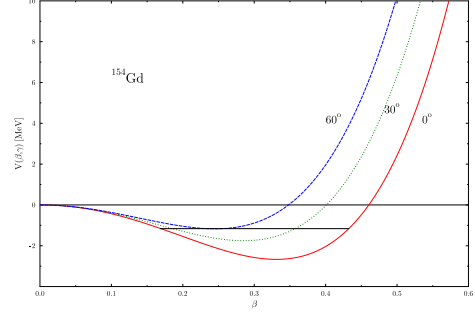


Figure 6.11: Projection of the GCM potential $V(\beta, \gamma)$ for ^{154}Gd [4, 51] with $\gamma = 0^\circ, 30^\circ$ and 60° . The position of the ground state is indicated by the horizontal line.

data, is indicated with a cross. It is evident that the ^{176}Os nucleus is very close to the parameters values which correspond to the X(5) symmetry.

6.3 The negative parity bands in ^{176}Os

The odd and even spins labeled with neg-1 and neg-2 in figure 5.3 are the yrast negative-parity states in ^{176}Os .

These bands were studied in the work [40]. The double-band structure of the neg-1 and neg-2 bands with negative parity is seen as a typical 2-quasiparticle configuration. A band with odd spins and negative parity starting at the $J^\pi = 7^-$ level is, in most of the cases, accompanied by a band with even spins and negative parity [43]. These bands are considered as signature of the same intrinsic excitation and have been observed in many nuclei e.g. the Barium and Xenon isotopes [43–47]. It has been found that for the lighter Os isotopes ($^{176,178}\text{Os}$) [40] the double band structure is a signature of the 2-quasiproton configuration with one proton in the $\pi_{\frac{5}{2}}[402]$ orbital coupled with a Coriolis mixed $h_{\frac{9}{2}}$ proton. Under the approximation of equation 6.1 it is possible to estimate the $\langle K^2 \rangle$ value of the band from the experimental $B(E2)$ values .

$$B(E2; I+2 \rightarrow I) = \frac{5}{16\pi} Q_0^2 \frac{3}{2} \frac{(I+1)(I+2)}{(2I+3)(2I+5)} \left(1 - \frac{\langle K^2 \rangle}{(I+1)(I+2)} \right)^2. \quad (6.1)$$

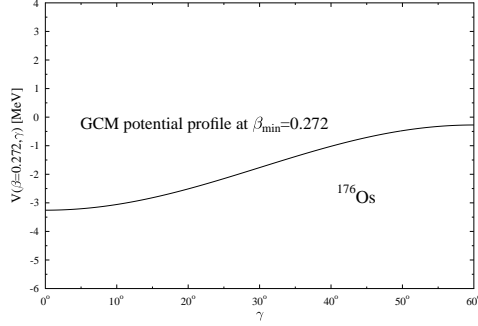


Figure 6.12: γ dependence of the GCM potential $V(\beta, \gamma)$ for ^{176}Os for β value corresponding to coordinates of the absolute potential minimum.

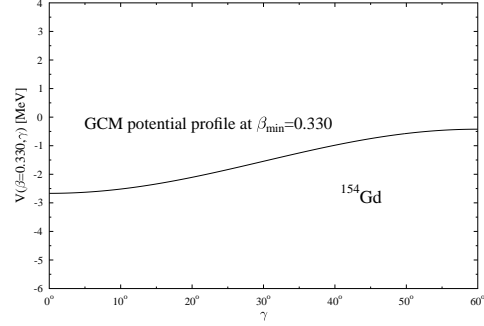


Figure 6.13: γ dependence of the GCM potential $V(\beta, \gamma)$ for ^{154}Gd [4, 51] for β value corresponding to coordinates of the absolute potential minimum.

In figure 6.14, the experimental $B(E2)$ reduced transition probabilities in the odd-spin negative parity band labeled with *neg-1* in ^{176}Os are compared to calculations performed at different $K_{rms} = \sqrt{\langle K^2 \rangle}$.

To reproduce the experimental values, a quadrupole momentum $Q_0 = 7.3\text{ eb}$ was used which is larger than to the Q_0 in the ground state band in ^{176}Os . The quasi-particle configuration underlying this band this band polarizes the nucleus to a bigger deformation.

In the suggested configuration [59] of the band, one proton is found in the $\frac{5}{2}[402]$ and for the other proton only the orbitals $\frac{1}{2}[541]$ and $\frac{3}{2}[532]$ are possible candidates. These configurations correspond to $K = 2$ and $K = 1$, respectively (see fig.6.14). Both the orbitals are deformation-driving and one expects larger deformation than in the ground state band. The high-j low- Ω intruder $\frac{1}{2}[541]$ proton with a rather large orbital moment drives the core to a large quadrupole deformation.

For these bands also a neutron configuration was taken as possible configuration [40], but it was found that for ^{176}Os the 2-quasineutron bands are at higher energy and hence for this nucleus these two bands can be identified to be 2-quasiproton configuration.

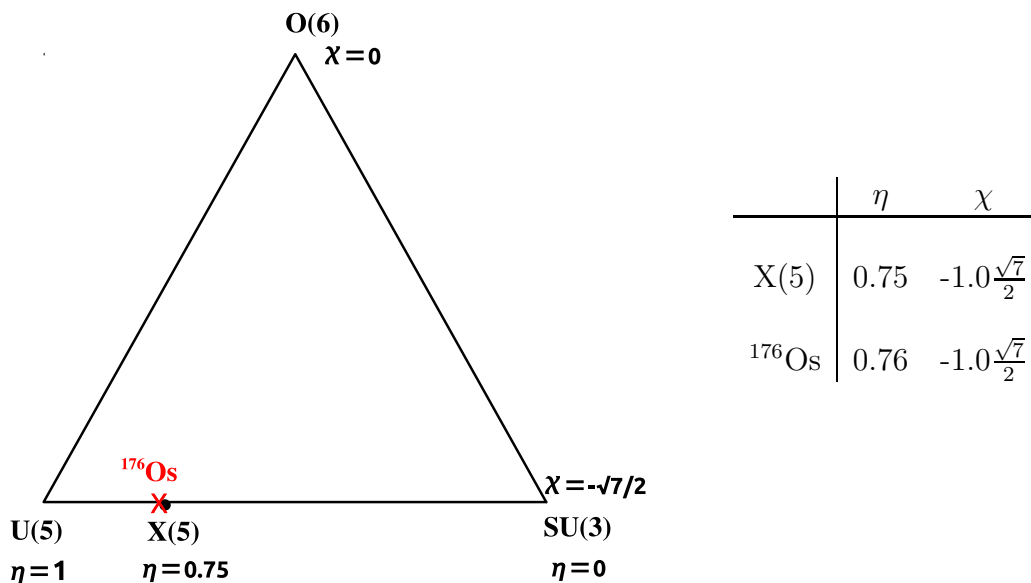


Table 6.8: Casten triangle for parameters of IBM-1. The position of the ^{176}Os nucleus is indicated. In the table the parameters of the IBM-1 fit for ^{176}Os as well as the parameters which correspond to the X(5) symmetry in the framework of IBM.

6.4 The rotational band in ^{177}Os

The lifetimes in a rotational band of ^{177}Os have been determined in this work and are reported in table 5.7. The lifetimes of the same levels have already been measured by O. Möller [51] and are consistent (see table 5.7) with the present values.

To describe the rotational band of ^{177}Os the Particle-Plus-Triaxial-Rotor Model is used [60]. The model is shortly described here. Bohr suggested to approximate the Hamiltonian of an odd-mass nuclear system with a hamiltonian which is the sum of the Hamiltonian of the doubly even core and an intrinsic Hamiltonian which contains a modified oscillator deformed single particle field and a BCS pair field. The single-particle energies and wave-

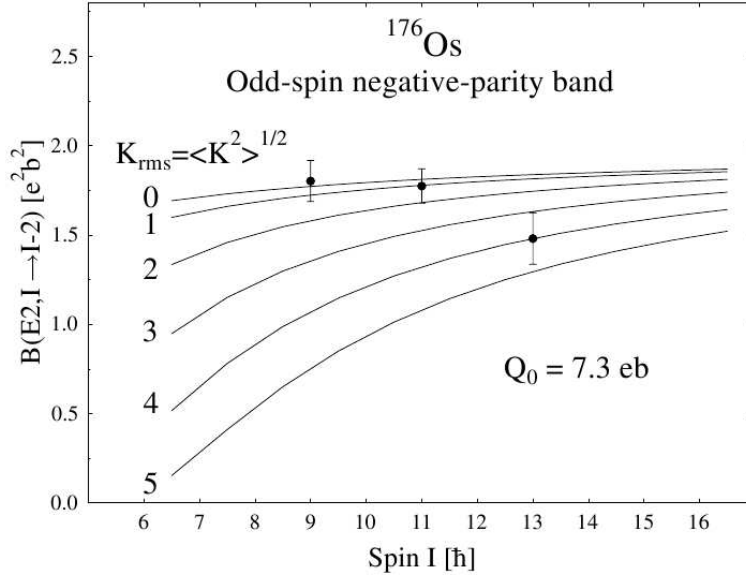


Figure 6.14: $B(E2)$ -values of intraband transitions within the negative parity band neg-1. The lines connect the values obtained by means of eq. 6.1 for fixed values of $K_{\text{rms}} = \sqrt{\langle K^2 \rangle}$.

functions in the modified oscillator are calculated for a given quadrupole deformation. In the first step of the calculation the single particle problem is solved for the odd nucleon in different Nilsson orbitals. The diagonalization of the intrinsic Hamiltonian is completed by means of a BCS transformation and the basis space is restricted to the one quasi particle states lying close to the Fermi level. In the second step the total Hamiltonian ($H_{\text{core}} + H_{\text{intrinsic}}$) is diagonalized in the set of symmetrized wave functions of the quasiparticle coupled to rotation. With these wave functions the electromagnetic matrix elements can be calculated. Based on this model calculations were performed to reproduce the electromagnetic matrix elements [51, 58] in ^{177}Os .

For the band under examination in the present work, the $\nu 1/2[521]$ -band (see fig. 6.15), the best agreement has been found for the deformation parameters set to $\beta = 0.26$ and $\gamma = 15.4^\circ$. The deformation parameter β has been deduced from the experimental E2 transition strengths. In figure 6.15 the comparison of the experimental results and the calculated ones is given. A good agreement has been found.

In table 6.9 the experimental $B(E2)$ values calculated from lifetimes in ^{177}Os measured in this work are compared to the experimental $B(E2)$ obtained in the work of O. Möller [51] and to the $B(E2)$ obtained by P. Petkov

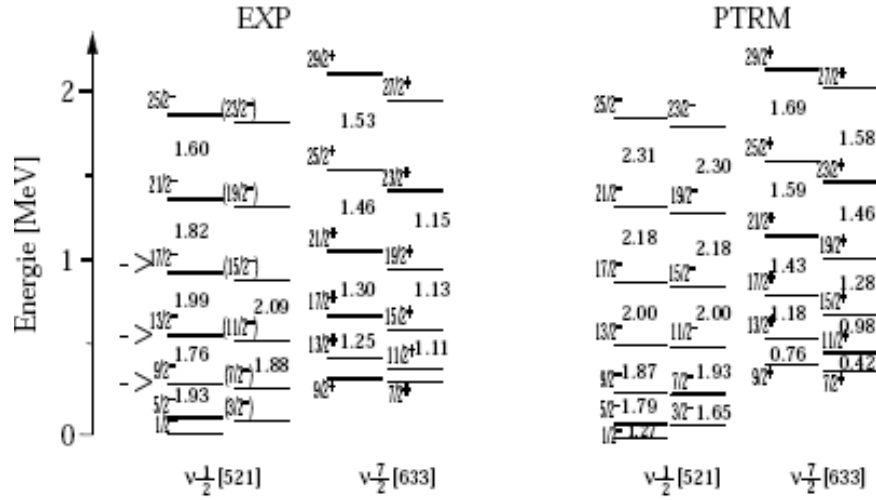


Figure 6.15: Comparison of the PTRM calculations performed by P. Petkov with the experimental data in ^{177}Os [51]. The $B(E2)$ values from [51] are given between the levels. The band under investigation in the present work is indicated with $\nu 1/2[521]$ and the levels observed are marked with arrows.

from PTRM calculations [51].

Table 6.9: Comparison of $B(E2)^\dagger$ in ^{177}Os obtained from the PTRM calculations made by P. Petkov with the experimental $B(E2)$ calculated from lifetimes derived in this work and the experimental $B(E2)^\ddagger$ obtained in [51].

I^π	Energy [keV]	E_γ [keV]	$B(E2)$ [e^2b^2]	$B(E2)^\dagger$ [e^2b^2]	$B(E2)^\ddagger$ [e^2b^2]
$\frac{9}{2}^-$	285.1	194.5	1.93(17)	1.79	1.93(16)
$\frac{13}{2}^-$	567.5	282.4	1.53(11)	1.87	1.76(14)
$\frac{17}{2}^-$	924.9	357.4	1.99(17)	2.00	1.99(15)

Conclusions

Up to now, for several of the nuclei in the mass region $A \approx 180$ only sparse data were known. In some cases the missing information or the big uncertainty of the known information did not allow to give a complete description of the nuclear structure. In the $^{176,178}\text{Os}$ isotopes spectroscopic information such as lifetime, transition probabilities etc. were not available before the experiments of this work. Only the lifetime of the first excited 2^+ state was measured. Very recently, lifetimes of high-spin in ^{176}Os have been measured using the Doppler shift attenuation method (DSAM).

The present work has enriched the experimental knowledge on the ^{176}Os osmium isotope by means of lifetime measurements with the plunger technique. The knowledge of the experimental lifetimes (i.e. the experimental transition probabilities) and of the experimental spectrum allows to extract information on the nuclear structure by comparison with theoretical models. In the present work new lifetimes have been measured in the ground state band up to the 12^+ state and in two side bands with negative parity in ^{176}Os . The lifetimes of the first excited 2^+ state, previously known with large uncertainties, were re-measured for $^{176,178}\text{Os}$ since this information was considered as a crucial parameter in the comparison with theory.

The experimental energies and $B(E2)$ transition probabilities in the fundamental sequence of ^{176}Os up to the 10^+ state follow the predictions of the $X(5)$ symmetry which characterizes nuclei at the critical point of the phase transition between spherical and axially deformed nuclei. The energy spacing of levels in the 0_2^+ sequence and the energy position of the 0_2^+ state are not well reproduced by the $X(5)$ model. The discrepancy observed between the experimental and predicted energies in the 2_3^+ sequence is smaller than 10%.

The experimental energies and $B(E2)$ transition strengths for the nucleus ^{176}Os were fitted with the IBM-1 and GCM models. These calculations provide a satisfactory interpretation of the structure of ^{176}Os .

The level scheme for the ground state band is described almost exactly in both fits. Discrepancies occur in the comparison with the experimental energies of the β and γ -bands. The energy spacing in both sequences are not

reproduced by the IBM-1 calculations. The IBM-1 reproduces the energies of the γ -band with a discrepancy smaller than 15%, while the energy spacing in the β -band for experimental data is lower. The energy spacing in the β and γ bands are quite well reproduced with the GCM model, however, the two band heads are at higher energies with respect to the experimental data. The intraband B(E2) transitions are well reproduced by the GCM predictions as well as the interband transitions for the β and γ band. The predicted IBM-1 B(E2) transition rates between states of the ground state band are underestimated within 20–40%.

A better agreement is obtained for the energies and B(E2) transition probabilities in the ground state band using the GCM compared with the IBM-1. However, it must also be considered that the comparison with GCM is based on a six parameters fit, which is four parameters more than for the IBM-1 model.

In this work, it was confirmed that the X(5) symmetry is a simple and good model which allows a direct comparison with the experimental data. Further advantage of the X(5) model is that it is nearly parameters free: the experimental level schemes can be described by direct comparison with the predicted energies and transition rates taking in consideration only two scaling factors. On the other hand, a more realistic interpretation of the experimental data could be made in terms of the IBM-2 model in which a distinction is made between protons and neutrons. In this framework an interpretation of M1 or E2/M1 transitions can be given.

It was shown in this work that the nucleus ^{176}Os is located inside the Casten triangle in the vicinity of the location which can be associated with the X(5) phase transition. Some of the characteristic features of the X(5) symmetry were demonstrated and the results obtained for the nucleus ^{176}Os are comparable in quality with those of well known X(5) nuclei in the mass region $A \sim 150$.

Further and future interest related to this work is focusing on the phase shape transitional region around the $A \approx 180$ where the features of the X(5) symmetry have been observed in the $^{176,178}\text{Os}$ nuclei. For example from energy ratios, the $^{176,178}\text{Pt}$ isotopes still show transitional behavior, although conclusive information from the lifetimes is still missing due to the missing information and (or) to the big uncertainty on the actually measured lifetimes.

Appendix A

Cascade calculation

CASCADE Calculation <small>L^AT_EX Output © F. Seiffert</small> <small>code vers.: F. Pühlhofer, Nucl.Phys.A 280(1977)267</small>										Target: 152Sm Projectile: 29Si		
Date of calc: 20091106		Compound Nucleus: 181Os						V _{coul.} = 123.14 MeV		L _{crit.} = 68ħ		
E [MeV]	ClO	ħ	142.00	144.00	146.00	148.00	150.00	152.00	154.00	156.00	158.00	160.00
Nuc.	chan.	σ / mb										
178Os	3n	6.03	3.95	2.48	1.43	0.78	0.35	0.08				
177Os	4n	197.80	171.29	138.67	105.48	75.84	51.49	33.62	21.24	12.97	7.71	
176Os	5n	143.90	180.20	209.47	230.35	239.28	232.81	217.31	187.87	154.20	120.91	
175Os	6n	8.00	14.70	24.92	35.17	46.50	64.04	79.68	107.67	126.61	144.53	
174Os	7n									5.86	10.37	
178Re	2np	0.50	0.27	0.09								
177Re	3np	25.80	24.77	22.41	18.90	14.85	10.95	7.58	4.92	3.03	1.74	
176Re	4np	14.54	18.83	23.07	27.15	31.66	33.45	33.37	31.70	28.16	23.87	
175Re	5np	4.05	6.74	10.49	15.13	19.45	25.58	33.58	41.32	46.92	52.54	
174Re	6np									2.56	3.98	
175W	2n α	1.19	0.84	0.55	0.31	0.13						
175W	4n2p					0.08	0.13	0.20	0.28	0.06	0.12	
174W	3n α	17.79	18.72	18.77	17.68	15.69	13.08	10.19	7.56	5.29	3.47	
173W	4n α	15.34	19.39	23.78	28.66	34.01	38.44	41.76	43.39	42.73	40.00	
172W	5n α	1.35	2.43	4.06	6.15	8.65	11.97	16.40	21.46	25.28	30.61	
171W	6n α									2.63	3.90	
175Ta	np α		0.01	0.02								
174Ta	2np α	0.51	0.86	1.31	1.81	2.20	2.39	2.36	2.09	1.68	1.23	
173Ta	3np α	0.54	1.30	2.62	4.57	7.12	10.20	13.50	16.68	19.43	21.45	
172Ta	4np α					0.11	0.38	0.93	1.87	3.20	5.20	
171Ta	5np α									0.03	0.19	
171Hf	2n2 α			0.15	0.36	0.57	0.72	0.77	0.70	0.56	0.40	
170Hf	3n2 α			0.28	0.70	1.37	2.29	3.39	4.61	5.70	6.52	
169Hf	4n2 α					0.05	0.26	0.62	1.21	2.05	3.37	
σ_{fusion}		464.87	508.62	550.68	591.38	630.68	668.54	704.98	740.45	773.59	804.78	
$\sigma_{fission}$		19.44	34.80	57.37	86.38	119.95	157.18	196.14	231.68	267.62	303.58	

Figure A.1: Cascade calculation [35] for the reaction $^{152}\text{Sm}(^{29}\text{Si}, 4n)^{176}\text{Os}$.

CASCADE Calculation <small>LaTeX Output © F. Seiffert</small> code vers.: F. Pühlhofer, Nucl.Phys.A 280(1977)267										Target: ^{164}Er Projectile: ^{16}O			
Date of calc: 20100615			Compound Nucleus: ^{180}Os				Vcoul. = 73.40 MeV		Lcrit. = 49ħ				
E [MeV]	ClO	ħ	76.00	78.00	80.00	82.00	84.00	86.00	88.00	90.00			
Nuc.	chan.		σ / mb										
^{178}Os	2n		8.16	11.64	11.67	10.12	7.75	5.50	3.62	2.27			
^{177}Os	3n		93.02	148.86	190.37	227.09	251.43	261.06	251.30	222.79			
^{176}Os	4n		5.43	25.60	57.24	90.66	130.69	179.99	241.80	297.90			
^{175}Os	5n									14.85			
^{178}Re	np		0.07	0.19	0.24	0.25	0.24	0.19	0.11	0.02			
^{177}Re	2np		4.77	8.89	12.84	16.29	19.24	21.85	23.77	24.32			
^{176}Re	3np		0.21	1.28	3.07	5.89	9.59	14.34	20.75	23.91			
^{175}Re	4np									7.87			
^{176}W	2n2p								0.11	0.02			
^{175}W	na		0.31	0.56	0.73	0.79	0.73	0.59	0.41	0.24			
^{174}W	2na		2.21	4.48	6.56	8.25	9.48	10.54	11.78	12.30			
^{173}W	3na		0.11	0.88	2.46	5.08	8.72	13.13	18.06	22.84			
^{172}W	4na									2.34			
σ_{fusion}			115.51	203.66	287.32	366.30	440.23	510.99	576.65	639.00			
σ_{fission}						0.01	0.09	0.38	1.02	2.15			

Figure A.2: Cascade calculation [35] for the reaction $^{164}\text{Er}(^{16}\text{O}, 4n)^{176}\text{Os}$.

CASCADE Calculation <small>LaTeX Output © F. Seiffert</small> code vers.: F. Pühlhofer, Nucl.Phys.A 280(1977)267										Target: ^{166}Er Projectile: ^{16}O			
Date of calc: 20100615			Compound Nucleus: ^{182}Os				Vcoul. = 73.18 MeV		Lcrit. = 49ħ				
E [MeV]	ClO	ħ	70.00	72.00	74.00	76.00	78.00	80.00	82.00	84.00	86.00	88.00	90.00
Nuc.	chan.		σ / mb										
^{180}Os	2n			0.16	1.13	2.14	2.44	2.32	1.89	1.46	0.97	0.61	0.34
^{179}Os	3n		0.18	4.69	34.09	80.91	118.80	141.99	153.12	154.02	142.61	121.90	96.68
^{178}Os	4n				7.34	38.69	83.59	139.43	199.98	266.13	339.24	356.85	397.42
^{177}Os	5n											58.78	94.71
^{179}Re	2np				0.56	2.24	3.89	5.23	6.28	7.14	7.72	7.81	7.26
^{178}Re	3np					0.49	1.82	3.71	6.27	9.44	13.47	15.32	17.90
^{177}Re	4np											3.67	7.52
^{177}W	na					0.05	0.14	0.15	0.13	0.09	0.01		
^{176}W	2na				0.26	1.40	2.55	3.29	3.77	4.04	4.33	4.46	4.40
^{175}W	3na					0.28	1.25	2.96	5.35	8.29	11.76	14.74	18.08
^{174}W	4na											1.23	2.79
σ_{fusion}			0.36	5.21	44.83	128.08	215.71	300.23	378.51	453.30	523.17	589.05	651.42
σ_{fission}									0.01	0.04	0.12	0.35	

Figure A.3: Cascade calculation [35] for the reaction $^{164}\text{Er}(^{16}\text{O}, 4n)^{176}\text{Os}$.

Appendix B

Lifetimes

Table B.1: Lifetimes of levels in the gsb of ^{176}Os at each ring–ring combinations. In the first column is indicated also in correspondence of which gate the data are referring. The label YYSH indicates that the gate is set on the shifted component of the transition YYY.

Gate	τ_{ring}	4+ 260.3 keV	6+ 347.0 keV	8+ 415.0 keV	10+ 476.3 keV	12+ 533.8 keV
347SH	τ_0	40.44(33)ps				
	τ_1	39.18(36)ps				
	τ_5	48.9(5)ps				
	τ_6	42.13(42)ps				
415SH	τ_1		9.20(16)ps			
	τ_5		8.29(15)ps			
	τ_6		8.47(15)ps			
415UN	τ_6			3.40(10)ps		
	τ_5			3.51(11)ps		
587SH	τ_0			3.44(11)ps		
	τ_1			3.21(10)ps		
	τ_5			3.88(12)ps	1.23(15)ps	
	τ_6			3.26(10)ps	1.18(22)ps	0.56(15)ps

Table B.2: Lifetimes of levels in the gsb of ^{176}Os . The lifetime τ_{corr} corrected for the slowing down of the recoils in the stopper material is reported.

I^π	Energy [keV]	E_γ [keV]	τ [ps]	τ_{corr} [ps]
4^+	395.5	260.3	40.4(6)	40.4(6)
6^+	742.3	347.0	8.56(30)	8.56(30)
8^+	1157.4	415.0	3.40(15)	3.40(15)
10^+	1633.8	476.3	1.20(20)	1.26 (21)
12^+	2167.8	533.8	0.56(22)	0.61(24)

Table B.3: Lifetimes of levels in the two negative parity bands of ^{176}Os at each ring-ring combinations.

Gate	τ_{ring}	9_1^+ 322.4 keV	11_1^+ 398.3 keV	13_1^+ 463.8 keV	
398SH	τ_0	7.69(36)ps			
	τ_1	7.03(36)ps			
	τ_5	7.54(31)ps			
464SH	τ_0		3.46(16)ps		
	τ_1		3.35(17)ps		
	τ_5		3.55(18)ps		
519SH	τ_6		3.39(19)ps	2.19(19)ps	
	τ_0				
	τ_1				2.2(2)ps
	τ_5				2.1(2)ps
	τ_6			1.9(2)ps	
Gate	τ_{ring}	8_2^+ 313.2 keV	10_2^+ 374.4 keV	12_2^+ 422.9 keV	
374SH	τ_0	6.7(7)ps	5.0(7)ps	4.7(3)ps	
423SH	τ_0				
477SH	τ_0				

Table B.4: Lifetimes of levels in the first and second excited band of ^{176}Os .

I^π	Energy [keV]	E_γ [keV]	I_γ	σ_γ	τ [ps]
9_1^-	2075.7	322.4	100 (3)	E2	7.7 (4)
		442.2	31 (5)		
		918.4	30 (3)		
11_1^-	2473.7	398.3	6.4(13)		3.5 (2)
		306			
		839.7			
13_1^-	2937.1	463.8	<14		2.2 (2)
		768.9			
8_2^-	2020.8	313.2	100(3)	E2	6.7 (7)
		863.1	33		
10_2^-	2394.8	374.4	100	E2	5.0(7)
12_2^-	2817.7	422.9	100	E2	4.7 (3)

Table B.5: Lifetimes of the first excited 2^+ of $^{176,178}\text{Os}$.

Nucleus	I^π	E_γ [keV]	τ [ns]	τ_{lit} [ns]	τ_{ee} [ns]
^{178}Os	2^+	132.4	1.02 (3)	0.99 (7)	1.05 (5)
^{176}Os	2^+	135.1	0.92 (13)	1.21 (18)	0.88 (3)

Table B.6: Measured lifetimes and transition probabilities in the ground state band of ^{176}Os .

I^π	Energy [keV]	E_γ [keV]	I_γ	σ_γ	τ [ps]	B(E2) [$e^2 fm^4$]	B(E2) [W.u.]
2^+	135.1	135.1	100	E2	920(130)	8451(287)	144(5)
4^+	395.5	260.3	100	E2	40.4(6)	14140(160)	243 (5)
6^+	742.3	347.0	100	E2	8.56(30)	17870 (150)	305 (11)
8^+	1157.4	415.0	100	E2	3.40(15)	18880^{+870}_{-800}	321^{+15}_{-14}
10^+	1633.8	476.1	100	E2	1.26(21)	25810^{+5160}_{-3690}	441^{+88}_{-63}
12^+	2167.8	533.8	100	E2	0.61(24)	30310^{+1970}_{-850}	517^{+336}_{-146}

Table B.7: Measured lifetimes of levels in ^{177}Os

I^π	Energy [keV]	E_γ [keV]	I_γ	σ_γ	τ [ps]	τ^\dagger [ps]
$\frac{9}{2}^-$	285.1	194.5	100	E2	110(9)	110(5)
$\frac{13}{2}^-$	567.5	282.4	100	E2	26.6(1.8)	23.3(9)
$\frac{17}{2}^-$	924.9	357.4	100	E2	6.6(5)	6.67(20)

Bibliography

- [1] F.Iachello Phys.Rev.Lett. 85,(2000)3580;
- [2] F.Iachello Phys.Rev.Lett. 87,(2000)3580;
- [3] O. Möller *et al.*, Phys.Rev C 72 034306(2005);
- [4] D. Tonev *et al.* Phys.Rev. C 69, 034334 (2004);
- [5] J. Jolie *et al.*, Phys. Rev. Lett. 89, 182502 (2002);
- [6] R. Krücken *et al.*Phys. Rev. Lett. 88(2002)232501;
- [7] R.Bijker *et al.*, Phys.Rev. C 68, 064304 (2003);
- [8] A. Dewald *et al.*, J. Phys. G: Nucl. Part. Phys. 31, S1427–S1432, (2005);
- [9] X. Hao *et al.* Chin.Phys. C 33, Supplement 1, 151 (2010);
- [10] I. Talmi, Simple model of complex nuclei, Harwood Ac. Publ. Gmbtt;
- [11] A. Bohr and B. R. Mottelson, Nuclear structure vol. I, II. W. A. Benjamin, New York, 1975;
- [12] G. Gneuss and W. Greiner, Collective potential energy surfaces and nuclear structure, Nucl. Phys A 171 449 (1971);
- [13] A. Arima and F. Iachello, Phys. Rev. Lett. 35 (1975)1069;
- [14] A. Arima and F. Iachello, Ann. Physy. 99 (1976) 253;
- [15] A. Arima and F. Iachello, Ann. Physy. 123 (1979) 486;
- [16] F.Iachello and A. Arima, The Interacting Boson Model, Cambridge University Press, Cambridge, 1987;
- [17] F. Iachello. Group Theoretical Method in Physics, Lecture Notes in Physics;

- [18] ; R. F.Casten and D. D. Warner, Rev. of Modern Physics, vol. 60, n. 2, 1988;
- [19] J.N.Ginocchio and M.R.Kirson, Nucl.Phys. A 350 31(1980);
- [20] P. Cejnar, J. Jolie and R. F. Casten, Quantum phase transitions in the shapes of atomic nuclei, to be published;
- [21] P.Cejnar and J.Jolie, Phys. Rev. E 58,387(1998);
- [22] L.D.Landau E.M.Lifshitz, Statistical Physics - Course of theoretical physics part one, 2000;
- [23] A. Dieperink, O. Scholten and F. Iachello, Phys. Rev.Lett. 44, (1980) 1747;
- [24] L. Fortunato, Eur. Phys.J., A 26, S01, I-30 (2005);
- [25] D. Bonatsos *et al.*, Phys. Rev. C 69, (2004) 014302;
- [26] D. J. Rowe, Nuc. Phys. A 735,(2004) 372 - 392;
- [27] M. A. Caprio, Phys. Rev. C 72, 054323 (2005);
- [28] See EPAPS Document No. E-PVRCAN-72-766511. This document can be retrieved via EPAPS homepage (www.aip.org/pubservs/epaps.html);
- [29] H. Morinaga, T. Yamazaki, In-beam Gamma-ray Spectroscopy; 406 (1976);
- [30] A. Dewald *et al.*, Z. Phys. A 334, 163 (1989);
- [31] G. Böhm *et al.*, Nucl. Instr. and Meth. A 329, 248 (1993);
- [32] P. Petkov *et al.*, Nuclear Instruments and Methods in Physics Research A457 (2001) 527 - 530;
- [33] ; G. Goldring, R. Bock(ed), HeavyIon Collisions, vol.3, North-Holland Publishing Company, Amsterdam, 1982, p.484;
- [34] D.Bazzacco and the GASP Collaboration, The gamma ray spectrometer GASP, Proc.Intern.Conf.on Nuclear Structure at high angular momentum, vol.2, (ottawa, 1992). Proceeding AECL 10613;
- [35] F. Pühlhofer, Nucl. Phys. A 280, 267 (1997);
- [36] S. Kasemann, unpublished;

- [37] J. Altmann, PhD thesis, University of Cologne (1994), unpublished;
- [38] B. Saha, program Napatau, Institut für Kernphysik der Universität zu Köln, 2002, unpublished;
- [39] G. F. Knoll, Radiation Detection and Measurement. John Wiley Sons, New York, 3-rd Ed.(1989);
- [40] G. D. Dracoulis, C. Fahlander, M. P. Ferrel, Nucl.Phys. A 383, 119 (1982);
- [41] P. Petkov *et al.*, Nuclear Instruments and Methods in Physics Research A431 (1999) 208 - 223;
- [42] B.Saha, Phys.Rev. C 70, 034313 (2004);
- [43] P. Petkov *et al.* Nucl. Phys. A 568, 572 (1994);
- [44] W. Gast *et al.*, Z. Phys. A 318, (1984)123;
- [45] K. Schiffer *et al.*, J. of Phys. G 15, (1989) L85;
- [46] P. Petkov *et al.*, Nucl. Phys. A 543 (1992) 589;
- [47] K. Loewenich *et al.*, Nucl. Phys. A 460 (1986) 361;
- [48] P. Petkov *et al.*, Nuclear Instruments and Methods in Physics Research A 349, 289 (1994);
- [49] T. K. Alexander and A. Bell, Nucl. Instr. and Meth. 81, 22-26 (1970);
- [50] J.M. Regis, Diploma thesis, unpublished;
- [51] O. Möller, PhD Thesis, unpublished (2005);
- [52] Agda Artna-Cohen, Nucl. Data Sheets, NNDC online data bank, National Data Center, Brookhaven, New York, USA;
- [53] Kibedi *et al.*, Nuc. Phys. A 383, 119-164 (1994);
- [54] M. A. Caprio, Phys. Rev. C 69, 044307 (2004);
- [55] D. Troltenier, J. A. Marhun and P. O. Hess, Computational Nuclear Physics, edited by K. Langanke, J. A. Marhun and S. E. Koonin (Springer, Berlin, 1991), p.105;
- [56] E. A. McCutchan and N. V. Zamfir, Phys. Rev. C 71, 054306, (2005);

- [57] A. Johnson, H. Ryde and J.Hjorth, Nucl.Phys. A 179, 753(1972);
- [58] P. Petkiv, private communication;
- [59] G. Dracoulis, C. Fahlander and M. P. Ferrel, Phys. Rev. Lett. 45, (1980) 1831;
- [60] S. E. Larsson, G. Leander and I. Ragnasson, Nucl. Phys. A 307, (1978) 189-223;
- [61] J. Jolie *et al.*, Phys. Rev. Lett. 87, 162501 (2001);
- [62] W. R. Leo, Techniques for Nuclear and Particles Physics Experiments, Springer-Verlag, 1994;

Acknowledgements

It is a pleasure for me to thank all the people to whom I am indebted for their help. Many thanks to:

Prof. Dr. Jan Jolie for his supervision, and for giving me the possibility to make this experience.

Dr. Alfred Dewald for having accepted me in the Plunger group, for teaching me all what I know about lifetime measurements, for the fruitful discussions and his precious help during the whole work at the IKP.

Dr. Oliver Möller, without him I would have never known how to get lifetimes, nice spectra etc... from raw data, for the nice time spent together during the experiments and during the long travels by car.

My best friend Dr. Antonella Scherillo, the “bridge” between me and the Cologne University, for having encouraged me in this experience and supported me in the difficulties, for listening me with patience each time i was complaining about something and for the fruitful discussions concerning nuclear physics.

Dr. Bart Bruyneel, for the friendship, the nice discussions during the lunch and tea time, for the careful reading of the manuscript, valuable comments and corrections, and for making me laugh with his Belgian sense of humor.

Dr. Christoph Fransen for the careful reading of the manuscript.

Dr. Pavel Petkov, for his precious help during my thesis work and for the nice discussions during the numerous “goodbye” parties.

My new group at the University of Florence, especially Prof. P. G. Bizzeti and Prof. A .M. Bizzeti for giving me the chance to work with them, Prof. A. Giannatiempo for her fruitful discussion about IBA calculations and Dr. A. Nannini for all the nice and interesting projects she involved me.

Dr. Olaf A. Thelen, for the stimulating discussions about German culture, politics and society, for been my personal “Information Office” with all the tips concerning “Leben als eine Kölnerin”.

Dr. Karl-Oskar Zell, without him the german burocracy would have killed me.

Dipl. Phys. Matthias Heidemann, for introducing me in the magic world of targets preparation, for his patience while i was trying to “fish the car-

bon foils” with small ”pinzette” and target frames and for showing me how produce good targets.

My friends Thomas, Denise, Chiara and Ayden Pissulla, one of the most beautiful family i have meet, for the daily help during my stay in Germany.

Dr. Irina Stefanescu for the friendship and her precious help in the first period of my stay in Cologne.

Dipl. Phys. Benedickt Birkenbach for his help with the translation of the abstract in German.

All the colleagues and friends of the IKP i have not mentioned for the nice atmosphere and the beautiful time spent together.

My friends Esther Hansen, Lynn and Nina Hansen and Chistian Thomé for the beautiful time spent together during the whole stay in Köln, the delicious dinners and for the funny time spent during our ”caffè letterari”.

My mother and my brothers for their love and support.

My husband, for having encouraged me, for his patience, his love and constant support.

My son Federico, for his love.

Erklärung

Ich versichere, dass ich die von mir vorgelegte Dissertation selbständig angefertigt, die benutzten Quellen und Hilfsmittel vollständig angegeben und die Stellen der Arbeit - einschließlich Tabellen, Karten und Abbildungen -, die anderen Werken im Wortlaut oder dem Sinn nach entnommen sind, in jedem Einzelfall als Entlehnung kenntlich gemacht habe; dass diese Dissertation noch keiner anderen Fakultät oder Universität zur Prüfung vorgelegen hat; dass sie - abgesehen von unten angegebenen Teilpublikationen - noch nicht veröffentlicht worden ist sowie, dass ich eine solche Veröffentlichung vor Abschluss des Promotionsverfahrens nicht vornehmen werde. Die Bestimmungen dieser Promotionsordnung sind mir bekannt. Die von mir vorgelegte Dissertation ist von Prof. Dr. Jan Jolie betreut worden.

Teilveröffentlichungen (kein)

Lebenslauf

Name Barbara Melon
Anschrift Via Valdossola 22, 40134 Bologna, Italien
Geburtsdatum/-ort 10.07.1972 in Torre del Greco Neapel, Italien
Nationalität italienisch
Familienstand/Kinder verheiratet, ein Sohn (3 Jahre)

Schulbildung:

77–82 Scuola elementare, Neapel, Italien
82–85 Scuola media statale “Angiolo Silvio Novaro”, Neapel, Italien
85–90 Liceo scientifico statale “Vincenzo Cuoco”, Neapel, Italien
16/07/90 Abitur

Hochschulstudium:

09/90 Immatrikulation an der Universität zu Neapel
für das Studienfach Physik
13/12/00 Diplom im Fach Physik mit dem Thema:
“Studio dei Canali di decadimento del
nucleo composto ^{87}Nb con l'apparato Euroball - Diamante
06/04 Beginn der Promotion, Fach Physik an der
Universität zu Köln

Arbeitsverhältnisse:

Seit 06/04-12/07 Wissenschaftliche Mitarbeiterin am
Institut für Kernphysik
der Universität zu Köln
Seit 11/09 Wissenschaftliche Mitarbeiterin am
Dipartimento di Fisica
Università degli Studi di Firenze

